https://doi.org/10.5194/hess-2019-391
Preprint. Discussion started: 20 August 2019

Hydrology and Earth System Sciences
Discussions

An Ensemble Square Root Filter for the joint assimilation of surface soil moiture and leaf area index within LDAS-Monde: application over the Euro-Mediterranean region

Bertrand Bonan[1], Clément Albergel[1], Yongjun Zheng[1], Alina Lavinia Barbu[1], David Fairbairn[2], Simon Munier[1], and Jean-Christophe Calvet[1]

[1]CNRM, Université de Toulouse, Météo-France, CNRS, Toulouse, France
[2]European Centre for Medium-Range Weather Forecasts, Reading, United Kingdom

Correspondence: Clément Albergel (clement.albergel@meteo.fr)

Abstract. This paper introduces an Ensemble Square Root Filter (EnSRF), a deterministic Ensemble Kalman Filter, to the context of assimilating jointly observations of surface soil moisture (SSM) and leaf area index (LAI) in the Land Data Assimilation System LDAS-Monde. By ingesting those satellite-derived products, LDAS-Monde constrains the Interaction between Soil, Biosphere and Atmosphere (ISBA) land surface model (LSM), coupled with the CNRM (Centre National de Recherches Météorologiques) version of the Total Runoff Integrating Pathways (CTRIP), to improve the reanalysis of land surface variables (LSVs). To evaluate its ability to produce improved LSVs reanalyses, the EnSRF is compared with the Simplified Extended Kalman, which has been routinely operated in LDAS-Monde, in a real case over the well-studied Euro-Mediterranean region at a 0.25º spatial resolution between 2008 and 2017. Both data assimilation approaches provide a positive impact on SSM and LAI estimates with respect to the model alone, putting them closer to assimilated observations. SEKF and EnSRF have a similar behaviour for LAI showing performances that are influenced by the vegetation type. For SSM, EnSRF estimates tend to be closer to observations than SEKF. The impact of assimilating SSM and LAI is also assessed on unobserved soil moisture in the other layers of soil. Unobserved control variables are updated in the EnSRF through covariances and correlations sampled from the ensemble linking them to observed control variables. In our context, a strong correlation between SSM and soil moisture in deeper soil layers is exhibited, as expected, showing seasonal patterns that vary geographically. Moderate correlation and anti-correlations are also noticed between LAI and soil moisture in spring, summer and autumn, their absolute value tending to be larger for soil moisture in root-zone areas, showing that assimilating LAI can have an influence on soil moisture. Finally an independent evaluation of both assimilation approaches is conducted using satellite estimates of evapotranspiration and gross primary production (GPP) as well as measures of river discharges from gauging stations. The EnSRF shows a systematic albeit moderate improvement for evapotranspiration and GPP and a highly positive impact on river discharges, while the SEKF exhibits a more contrasting performance.

https://doi.org/10.5194/hess-2019-391
Preprint. Discussion started: 20 August 2019

Hydrology and Earth System Sciences
Discussions

1 Introduction

Land surface variables (LSVs) are key components of the Earth system taking part, for example, in the water, vegetation and carbon cycles. Understanding their behaviour and simulating their evolution is a challenging task that has significant implications on various topics, from vegetation monitoring to weather prediction and climate change (Bonan, 2008; Dirmeyer et al., 2015; Schellekens et al., 2017). Land surface models (LSMs) play an important role in achieving these goals. Forced by atmospheric data and coupled with river-routing models, they aim to simulate LSVs such as soil moisture (SM), biomass and leaf area index (LAI). However, LSMs are prone to errors owing to innacurate initialisation, misspecified forcing and parameters or inadequate model physics. Another way to monitor LSVs is to use observations either from in situ networks or satellites. While in situ networks are generally sparse, remote sensing provides a global coverage of LSVs at spatial resolutions ranging from 25 km x 25 km to 300 m x 300 m but at a daily frequency at best (Lettenmaier et al., 2015; Balsamo et al., 2018). Also satellites do not observe every LSV such as root-zone soil moisture.

Combining observations with LSMs can overcome flaws of both approaches. This is the objective of Land Data Assimilation Systems (LDASs). Many of them focus on assimilating observations related to surface soil moisture (SSM), either using brightness temperatures, backscatter coefficients or soil moisture retrievals obtained from the two previous, to estimate soil moisture profiles (Lahoz and De Lannoy, 2014; Reichle et al., 2014; De Lannoy et al., 2016; Maggioni et al., 2017, and references therein). One popular approach has been the Simplified Extended Kalman Filter (SEKF). Introduced at Meteo-France by Mahfouf et al. (2009), it was initially designed for assimilating screen level observations to correct soil moisture estimates in the context of numerical weather prediction and is now involved in the operational systems of e.g. the European Centre for Medium range Weather Forecast (ECMWF, Drusch et al., 2009; de Rosnay et al., 2013) and UK Met Office. The SEKF has also been rapidly extended to the assimilation of soil moisture retrievals (Draper et al., 2009) and leaf area indices (Albergel et al., 2010; Barbu et al., 2011). Even though the approach has provided good results, it suffers from several limitations. It involves in particular the computation of a Jacobian matrix obtained by finite differences, meaning that one model run is required per control variable, thus limiting their number. That is why SEKF has been in competition with more flexible approaches such as the Ensemble Kalman Filter (EnKF) (Reichle et al., 2002; Fairbairn et al., 2015; Blyverket et al., 2019, among others) and particle filters (see e.g. Pan et al., 2008; Plaza et al., 2012; Zhang et al., 2017; Berg et al., 2019) for estimating soil moisture profiles. Those various approaches have been extensively compared in that context (Reichle et al., 2002; Sabater et al., 2007; Fairbairn et al., 2015).

LDASs are, however, not restricted to soil moisture. Recently monitoring vegetation dynamics through LDASs has gained attention. Defined as half the total area of green elements of the canopy per unit horizontal ground area, the LAI is a key land biophysical variable. One way to monitor LAI is to assimilate observations already used for surface soil moisture and link them to LAI. Both brightness temperature (see e.g. Vreugdenhil et al., 2016) and radar backscatter coefficient (Lievens et al., 2017; Shamambo et al., 2019, among others) are influenced by vegetation dynamics. This is the approach followed by Sawada et al. (2015) and Sawada (2018) who assimilate brightness temperatures using a particle filter to jointly estimate soil moisture profiles and LAI in the Coupled Land Vegetation LDAS (CLVLDAS).

https://doi.org/10.5194/hess-2019-391
Preprint. Discussion started: 20 August 2019

Hydrology and Earth System Sciences
Discussions

Another way to monitor LAI through LDASs is to assimilate observations of LAI. Satellite derived LAI products have benefited from recent advances in remote sensing (Fang et al., 2013; Baret et al., 2013; Xiao et al., 2013) and datasets are now available at the global scale and high resolution. While assimilating LAI has been done very often with crop models to estimate crop yields (see e.g. Pauwels et al., 2007; Ines et al., 2013; Jin et al., 2018), such assimilation has been, to our knowledge, seldom performed by LDASs. Jarlan et al. (2008) and Sabater et al. (2008) have succeeded introducing such approach in LDASs. The latter study has notably shown that assimilating jointly observations of SSM and LAI can improve the quality of root-zone SM estimates for one location in South West France. This work has been carried out with the CO2-responsive version of the Interactions between Soil, Biosphere and Atmosphere (ISBA) LSM (Calvet et al., 1998, 2004; Gibelin et al., 2006) developed by Meteo-France research centre (Centre National de Recherches Météorologiques, CNRM). This version of ISBA allows the simulation of vegetation dynamics including biomass and LAI. Stemming from that work, Albergel et al. (2010), Rüdiger et al. (2010) and Barbu et al. (2011) have introduced a SEKF assimilating jointly SSM and LAI and tested the approach on a site. This study has been extended to a series of locations over France (Dewaele et al., 2017) and to France (Barbu et al., 2014; Fairbairn et al., 2017) leading to LDAS-Monde (Albergel et al., 2017). Available through CNRM modelling platform SURFEX (SURFace EXternalisée, Masson et al., 2013), LDAS-Monde has been successfully applied to various parts of the globe: Europe and the Mediterranean basin (Albergel et al., 2017, 2019; Leroux et al., 2018), contiguous United States (Albergel et al., 2018b) and Burkina Fasso (Tall et al., 2019).

Lately other LDASs have started assimilating LAI using an EnKF assimilation approach. For example Fox et al. (2018) has assimilated LAI and biomass in order to reconstruct the vegetation and carbon cycles for a site in Mexico, and Ling et al. (2019) has compared various approaches for the assimilation of LAI at global scale. In addition Kumar et al. (2019) has assimilated LAI with an EnKF in the North American Land Data Assimilation System phase 2 (NLDAS-2) and studied its impact not only on vegetation but also soil moisture, water and carbon cycles, those LSVs being updated indirectly through the model using the updated LAI. Nevertheless these studies, contrary to LDAS-Monde, have not considered soil moisture estimation, i.e. no soil moisture variables were in the control vector.

This paper aims to develop an EnKF approach for the joint assimilation of LAI and SSM in LDAS-Monde. While the SEKF has been routinely employed in LDAS-Monde, an Ensemble Square Root Filter (EnSRF, Whitaker and Hamill, 2002), one of the many deterministic formulations of the EnKF (see e.g. Tippett et al., 2003; Livings et al., 2008; Sakov and Oke, 2008), has been proposed by Fairbairn et al. (2015) for the assimilation of SSM only in order to estimate soil moisture profiles. This study has also compared the performance of the EnSRF with the SEKF over 12 sites in South-West France. While performing better on synthetic experiments, the EnSRF provides results that are equivalent to the SEKF for real cases. Related to that work, Blyverket et al. (2019) uses another deterministic EnKF to assimilate SMAP satellite derived SSM over contiguous United States with the ISBA LSM focusing on soil moisture in the near surface while not updating root-zone soil moisture directly through data assimilation.

Building upon the work of Fairbairn et al. (2015), the present paper aims to (1) adapt the EnSRF to the joint assimilation of LAI and SSM within LDAS-Monde, (2) study the impact of assimilating LAI and SSM to LSVs using an ensemble approach, and (3) compare the EnSRF with the routinely used SEKF on its ability to provide improved LSV estimates. To achieve such

https://doi.org/10.5194/hess-2019-391
Preprint. Discussion started: 20 August 2019


Hydrology and Earth System Sciences
Discussions

goals, LDAS-Monde with EnSRF and SEKF is applied on the Euro-Mediterranean region (longitude from 11.5ºW to 62.5ºE, latitude from 25.0ºN to 75.5ºN, see Fig. 1 for the extent of the domain) for a 10 year experiment (from 2008 to 2017):

- using the vegetation interactive ISBA-A-gs LSM (Calvet et al., 1998, 2004; Gibelin et al., 2006) with the multi-layer soil diffusion scheme from Decharme et al. (2011),
- coupled daily with CNRM version of the Total Runoff Integrating Pathways river routing model (CTRIP, Decharme et al., 2019) to simulate hydrological variables such as river discharges,
- forced by the latest ERA-5 atmospheric reanalysis from ECMWF (Hersbach and Dee, 2016),
- and assimilating satellite derived Soil Water Index (SWI, as a proxy for SSM) and LAI products from the Copernicus Global Land Service (CGLS).

The performance of both DA approaches is assessed with (i) satellite-driven model estimates of land evapotranspiration from the Global Land Evaporation Amsterdam Model (GLEAM, Miralles et al., 2011; Martens et al., 2017), (ii) upscaled ground-based observations of gross primary production (GPP) from the FLUXCOM project (Tramontana et al., 2016; Jung et al., 2017), and (iii) river discharges from the Global Runoff Data Centre (GRDC). The paper is organised as follows: Sect. 2 details the various components involved in LDAS-Monde including the data assimilation schemes. Sect. 3 describes the experimental setup and the different datasets used in the experiment as atmospheric forcing, assimilated observations or for evaluation. The impact of the EnSRF on LSVs is then assessed in Sect. 4, including the comparison with the SEKF. Finally the paper discusses the issues encountered during the experiment and provides prospects in Sect. 5, before concluding in Sect. 6.

2 LDAS-Monde

LDAS-Monde (Albergel et al., 2017) is the offline, global scale and sequential data assimilation system dedicated to land surfaces developed by Meteo-France research centre CNRM. Embedded within the open-access SURFEX surface modelling platform (Masson et al., 2013, https://www.umr-cnrm.fr/surfex/), it consists of the ISBA land surface model coupled with the CTRIP river routing system and data assimilation routines that assimilates routinely satellite-based products of SSM and LAI to analyse and update soil moisture and LAI modelled by ISBA. The most recent SURFEX_v8.1 implementation is used to conduct our experiments. We quickly recall the main components of LDAS-Monde and subsequently detail the novel EnSRF approach for the joint assimilation of SSM and LAI. More information can be found in Albergel et al. (2017), see also https://www.umr-cnrm.fr/spip.php?article1022&lang=en.

2.1 ISBA land surface model

The ISBA (Noilhan and Planton, 1989; Noilhan and Mahfouf, 1996) LSM aims to simulate the evolution of LSVs such as soil moisture, soil heat or biomass. We use in this paper the soil multilayer diffusion scheme version (Boone et al., 2000; Decharme et al., 2011) involving a discretization of 14 layers of soil over 12 m depth to solve the mixed form of Richards equations

https://doi.org/10.5194/hess-2019-391
Preprint. Discussion started: 20 August 2019


Hydrology and Earth System Sciences
Discussions

(Richards, 1931) for water and the one-dimensional Fourier law for heat. The lower boundary of the 14 soil layers (0.01, 0.04, 0.1, 0.2, 0.4, 0.6, 0.8, 1.0, 1.5, 2.0, 3.0, 5.0, 8.0 and 12.0 m depth, see also Fig 1. of Decharme et al., 2013) was chosen to minimise errors coming from solving numerically the diffusion equations.

Regarding vegetation dynamics and interactions between water and carbon cycles, we use the ISBA-A-gs configuration (Calvet et al., 1998, 2004; Gibelin et al., 2006). This CO2-responsive version represents the relationship between the leaf-level net photosynthesis rate (A) and stomatal aperture (gs). Dynamics of vegetation variables such as LAI or biomass are induced by photosynthesis in response to atmospheric variations. LAI growing phase from a prescribed threshold (1.0 $m^2.m^{-2}$ for coniferous trees, 0.3 $m^2.m^{-2}$ for every other type of vegetation) results from an enhanced photosynthesis and CO2 uptake. On the contrary, a deficit of photosynthesis leads to higher mortality rates and a decreased LAI. Leaf biomass is determined from LAI (and vice-versa) through dividing LAI by the specific leaf area (one of the ISBA parameters depending on the vegetation type).

From a practical point of view, ISBA is run in this paper at a regular 0.25^o spatial resolution. Each ISBA grid cell is divided into 12 generic patches: 9 representing different types of vegetations (deciduous forests, coniferous forests, evergreen forests, C3 crops, C4 crops, C4 irrigated crops, grasslands, tropical herbaceous and wetlands), and three others depicting bare soils, bare rocks and permanent snow or ice surfaces. Each patch covers a varying percentage of grid cells. Denoted $\alpha_{[p]}$ for patch p of a given grid cell, this percentage is also known as the patch fraction. Vegetation and soil parameters for each patch and grid cell of ISBA are derived from the ECOCLIMAP II land cover database (Faroux et al., 2013) that is fully integrated in SURFEX.

2.2 CTRIP river routing model

The ISBA LSM is coupled with CTRIP to simulate hydrological variables at continental scale. Based originally on the work of Oki and Sud (1998), CTRIP aims to convert simulated runoff into river discharges. The model is fully described in the following papers: Decharme et al. (2010), Decharme et al. (2012), Vergnes and Decharme (2012), Vergnes et al. (2014) and Decharme et al. (2019).

CTRIP is available at a 0.5^o spatial resolution. Coupling between ISBA and CTRIP occurs on a daily basis through the OASIS3-MCT coupler (Voldoire et al., 2017). ISBA provides updated runoff, drainage, groudwater and floodplain recharges to CTRIP while the river routing model returns the water table depth or rise, floodplain fraction and flood potential infiltration to the LSM.

2.3 Data assimilation

LDAS-Monde is a sequential data assimilation system working on a 24h assimilation window. Each cycle is divided in two steps: forecast and analysis. Quantities produced during the forecast step (analysis step) are denoted with a superscript ^{f} (superscript ^{a}). The state of the studied system is described by $\mathbf{x}_{[p]}$ the control vector that contains every prognostic variable of the ISBA LSM for a patch p and a given grid point. In this paper, we consider LAI and soil moisture from layer 2 (1-4 cm depth) to 7 (60-80 cm depth) in the control vector, soil moisture in layer 1 being driven mostly by atmospheric forcings (Draper

https://doi.org/10.5194/hess-2019-391
Preprint. Discussion started: 20 August 2019


Hydrology and Earth System Sciences
Discussions

et al., 2011; Barbu et al., 2014). As in many LDASs, LDAS-Monde perform DA for each grid point independently (no spatial covariances considered).

The forecast step consists of propagating the state of the system from a time t to 24h later. Since patches and grid cells do not interact between each other in ISBA, denoted by $\mathcal{M}_{[p]}$ for patch p , the forecast step can be written as:

$$\mathbf{x}^f_{[p]}(t+24h) = \mathcal{M}_{[p]}\left(\mathbf{x}^a_{[p]}(t)\right) \tag{1}$$

The analysis step then corrects forecast estimates by assimilating observations of LAI and SSM.

2.3.1 Simplified Extended Kalman Filter

LDAS-Monde uses routinely a Simplified Extended Kalman Filter for the analysis step (Mahfouf et al., 2009). Observations (SSM and/or LAI) $\mathbf{y}^o$ are available at a grid cell level. To compute the analysis, we first need to calculate model equivalents of observations at the same level. This is performed by aggregating control variables from each patch to obtain the model equivalent $\mathbf{y}^f$ using a weighted average:

$$\mathbf{y}^f = \sum_{k=1}^{12} \alpha_{[k]} \mathbf{H} \mathbf{x}^f_{[k]} \tag{2}$$

$\mathbf{H}$ denotes the linear operator selecting model equivalent from each patch (modelled LAI for observed LAI, modelled soil moisture in layer 2 for SSM).

The SEKF analysis step then follows the traditional Kalman update, replaces the forecast error covariance matrix by a fixed matrix $\mathbf{B}$ and uses as observation operator the product of the model state evolution over the 24h window and the conversion of the model state into observation equivalents. We further suppose that the fixed $\mathbf{B}$ matrix is diagonal. This implies that there is no covariances between patches. In the end, for patch p it gives:

$$\mathbf{x}^a_{[p]} = \mathbf{x}^f_{[p]} + \alpha_{[p]} \mathbf{B} \left(\mathbf{H}\mathbf{M}_{[p]}\right)^T \mathbf{C}^{-1}_{\text{SEKF}} \left(\mathbf{y}^o - \mathbf{y}^f\right) \tag{3}$$

and

$$\mathbf{C}_{\text{SEKF}} = \sum_{k=1}^{12} \alpha^2_{[k]} \left(\mathbf{H}\mathbf{M}_{[k]}\right) \mathbf{B} \left(\mathbf{H}\mathbf{M}_{[k]}\right)^T + \mathbf{R} \tag{4}$$

with $\mathbf{R}$ the observation error covariance matrix and $\mathbf{M}_{[p]}$ the Jacobian matrix of $\mathcal{M}_{[p]}$. In practice, columns of $\mathbf{M}_{[p]}$ are calculated by finite differences using perturbed model runs. For each component x_j of the control vector and its perturbation δx_j, the j-th column of can be written as:

$$\left[\mathbf{M}_{[p]}\right]_j = \frac{\partial x^f(t+24h)}{\partial x_j} \approx \frac{\mathcal{M}_{[p]}\left(\mathbf{x}^a(t) + \delta x_j\right) - \mathbf{x}^f(t+24h)}{\delta x_j} \tag{5}$$

2.3.2 Ensemble Square Root Filter

We adapt the EnSRF from Whitaker and Hamill (2002) to the context of LDAS-Monde following the work of Fairbairn et al. (2015). The EnSRF is an EnKF-based approach in which the state of a system and associated uncertainties are described by an

https://doi.org/10.5194/hess-2019-391
Preprint. Discussion started: 20 August 2019

Hydrology and Earth System Sciences
Discussions

ensemble of N_e control vectors $\left\{\mathbf{x}_{[p]}^{(i)}, i = 1, \ldots, N_e\right\}$ for patch p of a given grid cell. The EnKF as a Monte Carlo approach approximates the classical Kalman Filter using the ensemble mean

$$\overline{\mathbf{x}}_{[p]} = \sum_{i=1}^{N_e} \mathbf{x}_{[p]}^{(i)} \tag{6}$$

to describe the state of the system and the ensemble covariance matrix

$$\mathbf{P}_{[p]} = \frac{1}{N_e - 1} \mathbf{X}_{[p]} \mathbf{X}_{[p]}^T \tag{7}$$

with $\mathbf{X}_{[p]} = \left[\mathbf{x}_{[p]}^{(1)} - \overline{\mathbf{x}}_{[p]}, \ldots, \mathbf{x}_{[p]}^{(N_e)} - \overline{\mathbf{x}}_{[p]}\right]$ the ensemble perturbation matrix, to describe the uncertainties of the estimation.

The forecast step is simple, we propagate as in Eq. (1) each ensemble member from a time to 24h later using the ISBA LSM. The analysis step then corrects the ensemble mean and the ensemble perturbation matrix by assimilating observations. To that end, we first calculate the model equivalent of observations by aggregating the mean of the forecast ensemble over all the patches

$$\mathbf{y}^f = \sum_{k=1}^{12} \alpha_{[k]} \mathbf{H} \overline{\mathbf{x}}_{[k]}^f \tag{8}$$

Then the EnSRF analysis creates an analysed ensemble whose mean and covariance matrix matches exactly the analysis of the Kalman Filter.

We choose to neglect here ensemble covariances between patches in the analysis step of the EnSRF. This asumption is in line with the succesfull methodology of the SEKF and ensures a fair comparison between both approaches. It also allows control variables from each patch to be updated independently. This places our approach in a similar context as others EnKFs involved in LDASs where ensembles with no more than 20 members have achieved satisfactory results. For example, Fairbairn et al. (2015) and Carrera et al. (2015) have shown that sampling errors from the finite ensemble size were not significant for ensembles greater than 20 members.

Following this asumption, for a given patch p the analysed mean and perturbation matrix are given by the following equations:

$$\overline{\mathbf{x}}_{[p]}^a = \overline{\mathbf{x}}_{[p]}^f + \alpha_{[p]} \mathbf{P}_{[p]}^f \mathbf{H}^T \mathbf{C}_{\text{EnSRF}}^{-1} \left(\mathbf{y}^o - \mathbf{y}^f\right) \tag{9}$$

and

$$\mathbf{X}_{[p]}^a = \left(\mathbf{I} - \alpha_{[p]} \widetilde{\mathbf{K}}_{[p]} \mathbf{H}\right) \mathbf{X}_{[p]}^f \tag{10}$$

with

$$\mathbf{C}_{\text{EnSRF}} = \sum_{k=1}^{12} \alpha_{[k]}^2 \mathbf{H} \mathbf{P}_{[p]}^f \mathbf{H}^T + \mathbf{R} \tag{11}$$

and

$$\widetilde{\mathbf{K}}_{[p]} = \alpha_{[p]} \mathbf{P}_{[p]}^f \mathbf{H}^T \left(\mathbf{C}_{\text{EnSRF}}^T\right)^{-1/2} \left(\mathbf{C}_{\text{EnSRF}}^{1/2} + \mathbf{R}^{1/2}\right)^{-1} \tag{12}$$

https://doi.org/10.5194/hess-2019-391
Preprint. Discussion started: 20 August 2019


Hydrology and Earth System Sciences
Discussions

Such an approach, contrary to the SEKF, updates the state covariance matrix that will evolve in time. This ensures that statistics of the estimates keep information from past observations.

3 Experimental setup and data sets

The effect of SEKF and EnSRF on LSVs is compared over the Euro-Mediterranean region (longitude from 11.5°W to 62.5°E, latitude from 25.0°N to 75.5°N) at a 0.25° spatial resolution during the decade 2008 – 2017. We detail in the following subsections the atmospheric forcing, the assimilated observations, the validation data sets employed in this comparison before detailing the experimental setup.

3.1 Atmospheric forcing

The ISBA LSM is forced with the ERA-5 atmospheric reanalysis (Hersbach and Dee, 2016) developed by ECMWF. ERA-5 reanalysis is available with an hourly frequency at a 31-km spatial horizontal resolution. To be used, surface atmospheric variables such as air temperature, surface pressure, solid and liquid precipitations, incoming shortwave and longwave radiations or wind speed are interpolated to ISBA 0.25° spatial resolution with a bilinear interpolation. Albergel et al. (2018a, b) have shown that forcing ISBA with ERA-5 compared to ECMWF previous ERA-Interim atmospheric reanalysis improves the quality of LSVs reanalyses.

3.2 Observations for assimilation

In this paper we assimilate observations from the SWI-001 and GEOV1 LAI data sets, both being distributed by the Copernicus Global Land Service . These satellite-derived products have been already successfully assimilated in LDAS-Monde (e.g. Leroux et al., 2018; Albergel et al., 2019).

The SWI-001 product consists of Soil Water Indices (SWI) obtained through a recursive exponential filter (Albergel et al., 2008) using backscatter observations from the ASCAT C-band radar (Wagner et al., 1999; Bartalis et al., 2007). A one-day time scale is used in the recursive filter in order to measure the wetness of the first centimetres of the soil. This product is available daily at a 0.1° spatial resolution. The raw SWI-001 averaged over the 2008-2017 period can be seen in Figure 1 (a).

To be assimilated, the SWI-001 product needs to be rescaled to the model climatology to avoid introducing any bias in the LDAS system (Reichle and Koster, 2004; Drusch et al., 2005). We apply a linear rescaling to SWI-001 to match the observation mean and variance to the mean and variance of the modelled soil moisture in the second layer of soil (1-4 cm). Introduced by Scipal et al. (2008), this rescaling also known as CDF (cumulative distribution function) matching is performed on a seasonal basis (with a 3-month moving window). Draper et al. (2009) and Barbu et al. (2014) have highlighted the importance of allowing seasonal variability in the rescaling.

The GEOV1 LAI product is obtained through a neural network algorithm (Baret et al., 2013) transforming observations of reflectance from SPOT-VGT and PROBA-V satellites into LAI. This dataset is available every 10 days at best at a one kilometre spatial resolution. The GEOV1 LAI averaged over the 2008-2017 period can be seen in Figure 1 (b).

https://doi.org/10.5194/hess-2019-391
Preprint. Discussion started: 20 August 2019


Hydrology and Earth System Sciences
Discussions

Following Barbu et al. (2014), both observation datasets are interpolated on the model grid (0.25° spatial resolution) where and when at least half of observation grid points are available. As in previous LDAS-Monde studies, we use a 24h assimilation window and observations are assimilated at 9:00 UTC.

3.3 Validation data sets

We consider independent datasets of evapotranspiration, gross primary production and river discharges to assess the validity of our approach and measure the influence of the EnSRF on the improvement of LSV reanalyses.

Satellite-derived estimates of evapotranspiration come from the GLEAM v3.3b product (Miralles et al., 2011; Martens et al., 2017). Daily estimates available for the period 1980 – 2018 at a 0.25° spatial resolution are fully driven by satellite observations and, as such, are independent from LDAS-Monde estimates. Figure 1 (c) displays GLEAM evapotranspiration averaged over the period 2008–2017 considered for validation in this paper.

Observations of Gross Primary Production (GPP) are derived from the FLUXCOM project. This dataset is obtained by merging upscaled measurements from eddy towers and satellite observations using machine learning. More details can be found in Tramontana et al. (2016) and Jung et al. (2017). They are available at a 0.5° spatial resolution on a monthly basis for the period 1982 – 2013. Figure 1 (d) shows FLUXCOM GPP averaged over the period 2008–2013 considered for validation in this paper.

River discharges obtained with CTRIP are compared to daily streamflow data from the Global Runoff Data Centre (https://www.bafg.de/GRDC). Due to the low resolution of CTRIP (0.5° spatial resolution), we only consider data for sub-basins with rather large drainage areas (greater than 10 000 km^2) with a long enough time series (4 complete years or more over 2008 – 2017).

3.4 Experimental setup

To assess the impact of EnSRF on LSV reanalyses and compare its efficiency with the routinely used SEFK, we have run LDAS-Monde over the Euro-Mediterranean region for the period 2008–2017 for three different configurations: one model run without assimilation (i.e. open loop), one using the SEKF and another one using the EnSRF with a 20-members ensemble. This size of the ensemble is consistent with Fairbairn et al. (2015) and Carrera et al. (2015). All three configurations start from the same initial state obtained after spinning-up ISBA-CTRIP twenty times over 2008. This provides an initial state for which the system has reached equilibrium.

For the SEKF configuration, the Jacobian matrix Eq. (5) is obtained by finite differences using perturbed model runs. Following Draper et al. (2009) and subsequent studies, perturbations are taken proportional to the dynamic range (difference between the volumetric field capacity w_{fc} and the wilting point w_{wilt}) for soil moisture variable. In practice they are set to $10^{-4} \times (w_{\mathrm{fc}} - w_{\mathrm{wilt}})$. For LAI, perturbations are set to following Rüdiger et al. (2010). Regarding the fixed background error covariance , we prescribe a mean volumetric standard deviation (SD) of 0.04 m^3.m^{-3} for soil moisture in the second layer and 0.02 m^3.m^{-3} for soil moisture in deeper layers, both are then scaled by the dynamic range. LAI background error SD is set

https://doi.org/10.5194/hess-2019-391
Preprint. Discussion started: 20 August 2019

Hydrology and Earth System Sciences
Discussions

to 20% of the LAI value for modelled values above 2.0 $m^2.m^{-2}$ and to a constant 0.4 $m^2.m^{-2}$ for modelled values below 2.0 $m^2.m^{-2}$. This SEKF configuration is the same as the successful one detailed in Albergel et al. (2017).

About the EnSRF configuration, the initial ensemble is obtained by perturbing the initial state using Gaussian perturbations with a zero-mean and using $\mathbf{B}$ for the covariance matrix. Ensemble Kalman Filters tend to underestimate variances and ensembles. This brings about an artificially shrunk spread leading ultimately to filter divergence if not counteracted. Hamill and Whitaker (2005) has shown that adding random perturbations to each ensemble member (additive inflation) at the start of each assimilation cycle can overcome this issue. It can also be used to represent model error. As in Fairbairn et al. (2015) we use time-correlated model errors using a first-order auto-regressive model. We prescribe an associated white noise with zero mean and a SD of $\lambda\,(w_{\rm fc} - w_{\rm wilt})$ for soil moisture (SM), with $\lambda = 0.5$ for SM in layer 2 (1-4 cm depth), 0.2 for SM in layer 3 (4-10 cm depth), 0.05 for SM in layer 4 (10-20 cm depth) and 0.02 for SM in deeper layers. These values are in line with Fairbairn et al. (2015). For LAI, we prescribe a white noise with zero mean and a SD of 0.5 $m^2.^{-2}$. We also fix the time correlation to 1 day for SM in the second layer and 3 days for SM in deeper layers. This is similar to Reichle et al. (2002) and Mahfouf (2007). For LAI, a rather small 1-day time correlation has to be used in order to avoid a collapse of the ensemble during the winter season due to the LAI threshold in ISBA.

For both SEKF and EnSRF configurations, we follow previous LDAS-Monde studies and set soil moisture observational errors to 0.05 $m^3.m^{-3}$ scaled to the dynamic range and LAI observational errors to 20% of the observed LAI values.

3.5 Evaluation strategy

As a sanity check, we first verify that EnSRF estimates of SSM and LAI are closer to observations than their model free run counterparts. We also compare the impact of EnSRF and SEKF on those two LSVs. This is achieved using scores such as biases, correlation coefficients (R), root mean square differences (RMSD) and normalised root mean square differences (nRMSD, RMSD divided by the averaged value of the studied variable).

The impact of assimilation on unobserved control variables (SM in deeper layers) is then assessed using daily analysis increment. Moreover, we study the evolution of ensemble correlations between unobserved and observed variables in the EnSRF configuration. They drive (as Jacobian values in the SEKF configuration) the influence of observations on unobserved control variables. We focus on SM in layer 4 (10-20 cm depth, SM4) and layer 6 (40-60 cm depth, SM6) as SM in layer 3 (4-10 cm depth) exhibits the same behaviour as SM4 and soil moisture in layer 5 (20-40 cm depth) and layer 7 (60-80 cm depth) have a similar response to SM6 (not shown).

Potential improvements on EnSRF and SEKF estimates for evapotranspiration and GPP are measured using the same metrics as for SSM and LAI.

Finally the influence on river discharges for both DA approaches is measured by the Nash-Sutcliffe efficiency (NSE) score:

$$\mathrm{NSE} = 1 - \frac{\sum_{t=1}^{T} (Q_t^s - Q_t^o)^2}{\sum_{t=1}^{T} \left(Q_t^o - \overline{Q}^o\right)^2} \tag{13}$$

https://doi.org/10.5194/hess-2019-391
Preprint. Discussion started: 20 August 2019


Hydrology and Earth System Sciences
Discussions

with Q_t^s the simulated or analysed river discharge at time t, Q_t^o the observed river discharge at the same time and $\overline{Q}^o$ the observed averaged river discharge. The NSE is a quantity between $-\infty$ and 1. A NSE value of 1 means that the model/analysis matches perfectly observations. A NSE value of 0 means that the model/analysis has the same accuracy as the observed averaged river discharge. Improvements or degradations caused by the SEKF or the EnSRF compared to the model run is measured with the Normalised Information Contribution Index (NIC):

$$\mathrm{NIC}_{\mathrm{NSE}} = 100 \times \frac{\mathrm{NSE}_{\mathrm{analysis}} - \mathrm{NSE}_{\mathrm{model}}}{1 - \mathrm{NSE}_{\mathrm{model}}} \tag{14}$$

4 Results

4.1 Impact of assimilation on LAI

Figure 2 displays for the model run, SEKF and EnSRF analyses and for observations, 10-days time series of LAI averaged over Europe and the Mediterranean basin spanning the period 2008 – 2017. It shows that the model simulation underestimates LAI compared to observations during winter and summer. The growing phase of vegetation occurs at a slower pace with averaged LAI reaching its maximum early August instead of late June – early July for observations. The senescence phase subsequently takes place later in the autumn compared to observations. Both data assimilation systems correct efficiently model simulations for that latter phase with EnSRF estimates getting closer to observations than SEKF ones. However, both SEKF and EnSRF fail to compensate the slower LAI dynamics of the model during spring. Nevertheless, both approaches reduce RMSD from 0.880 $m^2.m^{-2}$ for the model to 0.671 $m^2.m^{-2}$ for SEKF and 0.694 $m^2.m^{-2}$ for EnSRF and increase correlations with observations (from 0.593 for the model to 0.732 for SEKF and 0.723 for EnSRF). We also note that the maximum LAI for EnSRF is smaller than the model or the SEKF maxima. This is due in part to a systematic negative bias introduced by EnSRF model perturbations leading to an averaged bias of -0.201 $m^2.m^{-2}$ compared to a bias of -0.020 $m^2.m^{-2}$ for the model and -0.116 $m^2.m^{-2}$ for the SEKF.

Figure 3 shows nRMSD calculated over 2008 – 2017 for model outputs (a) and the difference between nRMSD for the model and the estimates produced with SEKF (b) and EnSRF (c). On average nRMSD is reduced from 0.57 (model) to 0.42 (EnSRF) and 0.40 (SEKF). Both assimilation approaches display the same geographical patterns reducing significantly nRMSD over most parts of the Euro-Mediterranean region (in blue in Figure 3). For example, roughly 20% of the domain has a nRMSD reduced by 0.25. We note that largest nRMSD reductions occur in places where nRSMD are large. The main differences between the two methods occur in Scandinavia, around the arctic circle, Ireland and Western Great Britain, where the SEKF shows greater positive impact than EnSRF, the latter even providing slightly degraded estimates compared to the model run for 3% of the total domain (in red in Figure 3 (c)).

The geographical patterns identified in Figure 3 can be explained in part by the type of vegetation covering grid cells. We investigate the impact of DA for each of the four main vegetation types encountered in the Euro-Mediterranean region: deciduous forests, coniferous forests, C3 crops and grasslands. To that end, we consider only grid cells (g.c.) in which at least 50% of their surface is covered by one of these vegetation types. Figure 4 displays the spatial distribution of those grid cells:

https://doi.org/10.5194/hess-2019-391
Preprint. Discussion started: 20 August 2019


Hydrology and Earth System Sciences
Discussions

1589 g.c. for deciduous forests (5.7% of the domain), 4223 g.c. for coniferous forests (15.2%), 1672 g.c. for C3 crops (6.0%) and 1725 g.c. for grasslands (6.2%).

We calculate the averaged seasonal RMSD for model outputs, SEKF and EnSRF analyses for the entire domain (Figure 5 (a)) and for each dominant vegetation type (Figure 5, (b)-(e)). The biggest impact of assimilating LAI occurs in autumn for deciduous forests (Fig. 5 (e)). For example, RMSD is reduced from 2.69 $m^2.m^{-2}$ for the model to 1.72 $m^2.m^{-2}$ for the SEKF and 1.45 $m^2.m^{-2}$ for the EnSRF. For C3 crops (Fig. 5 (c)) both assimilation approaches reduce RMSD in a similar manner, the largest decrease happening between August and October. The SEKF and the EnSRF offer contrasting performances in the case of grasslands (Fig. 5 (d)) as RMSDs are decreased by 0.18 $m^2.m^{-2}$ from model to SEKF estimates but by 0.09 $m^2.m^{-2}$ for EnSRF estimates. Strongest RMSD reductions occur in both cases in April and September. For coniferous trees (Fig. 5 (b)), neither SEKF nor EnSRF has an impact on RMSDs.

The scale of reduction in RMSD for EnSRF analyses is directly connected to estimated variances and standard deviations from the ensemble. The bigger the ensemble variances are, the larger are the weight of observations in the DA system. Figure 6 displays the seasonal evolution of ensemble standard deviations averaged over the whole domain and for grid cells dominated by one type of vegetation. Ensemble standard deviations are clearly larger in summer than in winter peaking in July for c3 crops at 0.22 $m^2.m^{-2}$, in August for grasslands at 0.14 $m^2.m^{-2}$ and in September for coniferous forests at 0.07 $m^2.m^{-2}$. The maximum standard deviation is observed for deciduous forests and reaches 0.35 $m^2.m^{-2}$ also in September.

4.2 Impact of assimilation on SSM

This section studies the impact of assimilating jointly LAI and SSM on estimated SSM. We firstly recall that observed SSM is derived from the SWI-001 satellite product and is matched to the model climatology of soil moisture in the second layer of soil (1-4 cm depth) using a seasonal CDF matching. This means that assimilating observed SSM mostly corrects the short-term variability of estimated SSM and does not modify its climatological seasonal cycle. Results from either SEKF or EnSRF experiments are in line with this statement. For example, the bias between observed and estimated SSM remains, on average over 2008-2017, below 0.002 $m^3.m^{-3}$ all over the domain.

Figure 7 displays RMSD calculated over 2008 – 2017 for model outputs (a) and the difference between RMSD for the model and the estimates produced with SEKF (b) and EnSRF (c). On average, RMSD is reduced from 0.035 $m^3.m^{-3}$ (model) to 0.032 $m^3.m^{-3}$ (SEKF) and 0.027 $m^3.m^{-3}$ (EnSRF). Model RMSD tends to be generally larger in wetter places than in drier places with the exception of South East Spain and parts of Northern Africa where RMSDs can be larger than 0.050 $m^3.m^{-3}$. Both assimilation approaches reduce significantly RMSD in many places over the domain (in blue in Figure 7 (b-c)). The main reduction occurs for both approaches in the southern part of the Euro-Mediterranean region where grid cells consists of bare soil and bare rocks. In those places, vegetation is sparse, and SSM is the main source of information in assimilated observations making its impact more straightforward. We also notice that the EnSRF tends to produce estimates that are closer to observations than SEKF estimates.

Assimilation also improves correlations with observed SSM from 0.544 for model outputs in average to 0.652 for the SEKF and 0.760 for the EnSRF. Figure 8 illustrates correlations for model outputs (a) and difference between correlations for the

https://doi.org/10.5194/hess-2019-391
Preprint. Discussion started: 20 August 2019


Hydrology and Earth System Sciences
Discussions

model and SEKF (b) and EnSRF (c) outputs. From correlation results, similar conclusions are drawn as from RMSDs. In particular the main improvement occurs in Northern Africa for both approaches. Finally we observe negative correlations between model outputs and observed SSM in arid places such as deserts in Sahara and the Arabian Peninsula.

4.3 Correlations between observed and unobserved control variables

Examining Jacobians in the SEKF has provided interesting insights on the sensitivity of SSM and LAI on soil moisture in deeper layers (see e.g. Albergel et al., 2017, covering the Euro-Mediterranean region between 2000 and 2012). In the EnSRF, the role of Jacobian is devolved to correlations sampled from the ensemble covariance matrix. Figure 9 shows maps of correlations between soil moisture in layer 2 (1-4 cm depth, SM2 used as a proxy for SSM) and SM in layer 4 (10-20 cm depth, SM4) and layer 6 (40-60 cm depth, SM6) and correlations between LAI and SM2, SM4 and SM6. Correlations are averaged by season (December-January-February, March-April-May, June-July-August and September-October-November) over the whole 2008 – 2017.

The first two rows of Figure 9 show the seasonal evolution of correlations between SM2 and SM4 and SM6. SM4 is highly correlated to SM2 (in blue), R being above 0.5 for most places of the domain for each season and correlations with SM2. SM6 is also highly correlated to SM2 but to a lesser extend meaning that correlations with SSM decrease in absolute value when we reach deeper soil layers. We also notice seasonal tendencies. For example, correlations with SM2 tend to be larger in Western Europe during Spring while they reach their maximum during Summer in Scandinavia. Negative correlations with SM2 (between -0.35 and -0.20) tend to appear during Winter over Russia. It means that in those areas in winter, there is less liquid water in the surface when there is more liquid water in deeper layers. This is linked to snow and freezing as we only compare liquid soil moisture from the different layers of soil. We further notice that SM2 and SM6 are uncorrelated in Summer over Spain and Northern Africa. Finally we remark that in very arid places such as in Sahara SM2 is not correlated to soil moisture in deeper layers (either SM4 and SM6). This implies that assimilating SSM in those areas will not modify soil moisture in deeper layers as we will show in the next section.

The last three rows of Figure 9 show the seasonal evolution of correlations between LAI and soil moisture in layers 2, 4 and 6. Soil moisture tends to be less correlated on average to LAI than to SSM nevertheless the values reached are relatively large (between -0.5 and 0.5). It means that assimilating LAI has an impact on estimated soil moisture. In detail, correlations between LAI and SM6 are larger in absolute value than with SM4 and with SM2 meaning that LAI is more correlated to root-zone soil moisture than with SSM. We also observe seasonal geographical patterns. Positive correlations tend to appear in Summer in Northern Europe where deciduous and coniferous forests are dominant meaning more water in the soil leads to a greater LAI. On the contrary in Spring and Summer, negative correlations appear around the Mediterranean basin.

4.4 Impact of assimilation on soil moisture in deeper layers

Figure 10 displays soil moisture for layers 4 and 6 averaged over 2008 – 2017 from the model (left) and the averaged difference with SEKF estimates (central panels) and EnSRF estimates (right). We observe that the SEKF has the same averaged SM4 as the model. Nevertheless we discern seasonal tendencies. Figure 11 shows analysis increments for SM4 and SM6 for SEKF

https://doi.org/10.5194/hess-2019-391
Preprint. Discussion started: 20 August 2019


Hydrology and Earth System Sciences
Discussions

(top row) and EnSRF (bottom row) for May, July and September. We see that increments on SM4 tend to be negative in May and September in most parts of the domain and positive in July in Northern Europe for SEKF. EnSRF estimates for SM4 tends to be similar to SEKF estimates. The main difference occurs in Northern Africa and in the Arabian peninsula where the soil is estimated wetter than in SEKF with a difference reaching 0.02 $m^3.m^{-3}$. This disparity over arid zones in due solely to a wet bias introduced by model error as assimilating SSM in those places has no influence due to negligible correlations between SSM and SM4. We also identify greater EnSRF SM4 estimates over places such as Poland and Spain but the difference, being always below 0.01 $m^3.m^{-3}$, comes from more positive increments during the summer period (as shown for July in Figure 11). Except in arid areas, SM4 estimates and analysis increments for SEKF and EnSRF tend to be similar, thus, making our SM4 estimates less dependant on the data assimilation method.

Regarding SM6 estimates, both SEKF and EnSRF produce a drier soil layer than the model for most of the domain as shown in Figure 10. We identify these patterns for every month without any seasonality (not shown). For SEKF drier estimates are obtained through cycling as analysis increments are close to zero. For EnSRF, cycling is also responsible to this drying but analysis increments are not negligible (-0.01 $m^3.m^{-3}$ for biggest values) and compensate the wet bias from model error in SM6 (not shown). As for SM4, SM6 EnSRF estimates are larger than SEKF and model estimates in Northern Africa, but this time only for places where bare soil dominates as for places where bare rocks dominates the soil dries due to cycling. Again assimilation does not modify directly estimates as correlations are null.

Overall SEKF and EnSRF provide similar estimates for soil moisture in deeper layers for most places but not necessarily through the same mechanisms.

4.5 Evaluation using Evapotranspiration and Gross Primary Production

We now evaluate the performance of our data assimilation systems using independent satellite-based datasets of evapotranspiration (ET) and gross primary production (GPP).

The model tends to underestimate ET leading to an averaged negative bias of -0.328 $kg.m^{-2}.day^{-1}$ reaching -0.8 $kg.m^{-2}.day^{-1}$ in June and July. Both SEKF and EnSRF reduce this bias to -0.114 $kg.m^{-2}.day^{-1}$ and -0.059 $kg.m^{-2}.day^{-1}$, respectively. Figure 12 displays correlations between the GLEAM dataset and model estimates (a) and the difference between correlations for the model and the estimates produced with SEKF (b) and EnSRF (c). Overall the correlation is increased on average from 0.789 to 0.803 (SEKF) and 0.823 (EnSRF). EnSRF provides estimates that are more correlated with this independent dataset for almost everywhere, it improves correlation (between 0.05 and 0.1) especially over Spain, Northern Africa or around the Caspian Sea where correlations between the model and GLEAM were poorer than for the rest of the domain, showing its positive impact on ET. Similar conclusions can be drawn from geographical patterns observed for RMSD and nRMSD (not shown, see Table 1 for averaged results).

Figure 13 depicts correlation between GPP from the FLUXCOM dataset and model estimates (a) and the difference between correlations for the model and the estimates produced with SEKF (b) and EnSRF (c). As for ET, the EnSRF provides GPP estimates that are more correlated to the FLUXCOM dataset than model and SEKF estimates for almost everywhere, on average 0.817 compared to 0.784 for the model and 0.786 for the SEKF. The best improvements are noticeable on around the

https://doi.org/10.5194/hess-2019-391
Preprint. Discussion started: 20 August 2019


Hydrology and Earth System Sciences
Discussions

Caspian Sea (above 0.05) where correlations between the model and FLUXCOM GPP were poorer than for the rest of the domain. Also contrary to the SEKF, degradations are confined to only few places in Iraq, Iran and close to the Arctic circle. Again similar conclusions can be drawn from geographical patterns observed for RMSD and nRMSD (not shown, see Table 1 for averaged results).

Overall the EnSRF exhibits moderate improvements for GPP and ET compared to SEKF, thus validating our approach.

4.6 Evaluation using river discharges

We limit our evaluation to 92 stations over Europe with a model NSE above -1. The NIC of EnSRF compared to the model is displayed for those stations in Figure 14. Most stations are located in France and Germany. Blue circles denote a positive impact (above 3%) of EnSRF on estimated river discharges, red circles a negative one (below – 3%) and grey diamonds a neutral impact (between –3% and 3%). A positive NIC is observed for 61 stations and a negative NIC for only 11 stations. Largest NIC are noticed for German stations. Such a positive influence for EnSRF constrasts with the rather neutral effect of SEKF on river discharges. In compliance with previous studies (Albergel et al., 2017; Fairbairn et al., 2017), we observe a significantly positive NIC of SEKF for only 15 stations and a negative NIC for 3 stations (not shown).

5 Discussion

5.1 Is the EnSRF able to provide improved estimates of LSVs?

Section 4 shows overall the ability of the EnSRF to provide improved LSVs reanalyses when LAI and SSM are assimilated jointly.

For LAI, EnSRF estimates are on average as close as SEKF estimates to observations. We notice a stronger impact of both data assimilation approaches during the senescence phase than during the growing phase. This is in compliance with what Albergel et al. (2017) and Leroux et al. (2018) have observed over the Euro-Mediterranean region. During the growing phase, the system can artificially add LAI and biomass, but if atmospheric conditions are not favourable, the modelled biomass cannot maintain its growing rate. During the senescence, LAI dynamics is driven by the rate of mortality, thus making DA more efficient. We further notice that DA has an impact that varies with the type of vegetation. Impact tends to be larger when the vegetation is dominated by deciduous forests. On the contrary, neither SEKF nor EnSRF has an impact on LAI for coniferous forests. But the model perfoms well on places where more than 50% of plants are coniferous trees and LAI dynamics is weak in those places. Finally we observe that the EnSRF introduces a negative bias in LAI estimates compared to model or SEKF counterparts. This bias is caused by the ensemble perturbations coming from the model error. As pointed out by Fairbairn et al. (2015), model error can introduce a bias into the system in LDASs, thus showing its influence.

In the case of LAI, model errors applied to LAI in every vegetation patch are sampled from the same distribution. However, the behaviour of ensemble standard deviations varies greatly seasonally and for each type of vegetation. Standard deviations for coniferous trees are so low it leads to almost no impact of DA. Such behaviour can be explained by two caveats: first, ISBA

https://doi.org/10.5194/hess-2019-391
Preprint. Discussion started: 20 August 2019


Hydrology and Earth System Sciences
Discussions

modelled LAI evolves over a prescribed threshold (1 $m^2.m^{-2}$ for coniferous forests, 0.3 $m^2.m^{-2}$ for other vegetation patches). When perturbed using model error, estimated LAI can be below this threshold. To avoid model issues, estimated LAI is reset to that threshold when it is the case leading to an artificially reduced ensemble standard deviation when modelled LAI is close to that threshold as in winter. Secondly, since LAI dynamics are smooth, reduced ensemble standard deviations due to the winter season still have an impact in spring through cycling. Overall we observe that ensemble standard deviations for LAI highly depend on the type of vegetation. An approach for model errors tailored for each vegetation patch could overcome the observed caveats.

Regarding SSM, EnSRF estimates tend to be closer to observations than SEKF estimates. This behaviour is systematic and is due to the prescribed model error for the EnSRF and the prescribed background error covariance matrix in the SEKF. We put more uncertainty in the additive model error as we are unsure of our approach compared to the background error covariance matrix that has been routinely used in the SEKF. We also observe that in arid places such as the Sahara, observed and modelled SSM are negatively correlated even after CDF match. This shows that the short-term variability of observations is completely different from what we model in ISBA. It raises the question of the quality of ISBA and/or SSM observations (after CDF matching) in arid places. Stoffelen et al. (2017) has shown that observed SSM derived from scatterometers can have a poor quality in arid places. Studying further such aspects is however beyond the scope of the paper.

About soil moisture in deeper layers, both approaches tend to provide similar estimates excepted in arid places where the EnSRF provides a wetter soil than the SEKF. This difference is solely due to a wet bias introduced again by the model error. When we perturb soil moisture, we ensure that soil moisture remains positive. In arid places where soil moisture is really low, perturbations fatally add water. As soil moisture in deeper layers is not correlated to SSM or LAI in those places, DA cannot correct this bias using observations of SSM or LAI. In other places, the EnSRF can correct the bias potentially introduced by model error to unobserved control variables through the help of correlations. They give insightful information on how the system works. Conclusions drawn from correlations are in accordance with those derived from the analysis of SEKF Jacobians drawn in Albergel et al. (2017) over the Euro-Mediterranean region and Tall et al. (2019) over Burkina-Fasso. We further remark that in dry places in Summer, negative correlations between LAI and soil moisture appear. This means a higher LAI leads to a reduced soil moisture due to plant transpiration in part. Barbu et al. (2011) has already highlighted this kind of behaviour for Jacobians for grassland places in South-West France. Correlations explain the links between variables in ISBA LSM. However, they are influenced by the way we apply model error. Another model error, perturbing for example atmospheric forcing, may have led to different correlations.

Section 4 shows that EnSRF provides also improved estimates for evapotranspiration, gross primary production and river discharges. In the case of river discharges, their rather systematic improvement may be due in part to the assimilation of SSM and LAI. It may also be due in part to a bias added by the EnSRF ensemble formulation (as observed for other LSVs) that compensates an existing bias due to the coupling between ISBA and CTRIP. Further investigations have to be conducted to explore this question (out of scope). Moreover, a negative NIC is observed for most Spanish stations, where anthropogenic effects (irrigation, importance of dams, ...) dominate hydrological cycles. Since CTRIP does not consider anthropogenic effects, this can explain poor performances of the LDAS-CTRIP system.

https://doi.org/10.5194/hess-2019-391
Preprint. Discussion started: 20 August 2019


Hydrology and Earth System Sciences
Discussions

5.2 How to deal with model errors in LDAS-Monde EnSRF?

As seen in the previous section, the quality of EnSRF estimates highly depends on the specified model error. We have seen that our system would benefit from a more tailored approach. One way that has been followed in the LDAS community is to use perturbed atmospheric forcings to generate an ensemble of more physical states. This can be done by either perturbing precipitations only (e.g. Fairbairn et al., 2015; Munier et al., 2015), operating a more complex system of perturbations that includes correlations between precipitation, short wave and long wave radiations (see among others Reichle et al., 2007; Liu et al., 2011; Kumar et al., 2014). Another possibility is to perturb land parameters such as the soil texture (Blyverket et al., 2019) or vegetation parameters. The main drawback of such approaches is that they tend to overcome underestimated ensemble variances by putting too much uncertainty on atmospheric forcings or model parameters that might be far better known than assumed. They can also induce a bias in model estimates (as shown by Fairbairn et al., 2015).

Model error in Ensemble Kalman Filters aims to compensate insufficiencies of the model and forcings but is difficult to prescribe as it aims to compensate something we do not know. One way to curb this issue is to estimate model error. Dee (2005) describes a range of approaches to account for model biases in data assimilation systems. The last decade has also seen the development of techniques to estimate model error covariance matrices (see Tandeo et al., 2018, for a review of existing approaches). Approaches based on Desroziers diagnostics (Todling, 2015; Bowler, 2017) or on statistics of consecutive innovations (Berry et al., 2013; Harlim et al., 2014) seem affordable for LDASs from a computational point of view.

All these approaches help to estimate model deficiencies but do not necessarily provide the reasons of those caveats. For land surface models, they can come not only from possibly inadequate atmospheric or soil and vegetation parameters but also from inadequate model physics (missing processes, ...). Finding the reasons of those is a complex task. An interesting step would be to assess the influence of atmospheric uncertainties on LSMs by using ensemble atmospheric forcings such as the 10-members atmospheric reanalysis included in ERA5 (available at a coarser spatial and temporal resolution though) or the 51 members of ECMWF ensemble medium-range forecasts. Such idea has been explored over Spain in the case of multi-models and multi-forcings ensembles by Ehsan Bhulyan et al. (2019).

5.3 The question of cross-covariances

Both SEKF and EnSRF in this paper do not consider covariances between patches and between grid cells. However, those covariances are likely to exists. For example, each patch of a given grid cell is forced with the same atmospheric forcing, errors in the forcing would result to correlated errors for the state of each patch. The same thing could be said for the state of two neighbouring grid cells since errors in atmospheric reanalyses are spatially correlated. Including those covariances could be beneficial to LSV reanalyses.

By construction, the SEKF cannot include these covariances. Indeed the SEKF relies on the ISBA land surface model to calculate covariances between variables. Since each patch of each grid cell of the model run independently, it cannot create covariances between patches or between grid cells.

https://doi.org/10.5194/hess-2019-391
Preprint. Discussion started: 20 August 2019


Hydrology and Earth System Sciences
Discussions

On the contrary, Ensemble Kalman Filters can include this information automatically as estimated covariances are built from the ensemble, thus making EnKFs more flexible than the SEKF. In our case, that would lead to a single state vector containing the LAI and SM in the various layers of soil of each patch and multiply by around 12 the size of this state. Fairbairn et al. (2015) and Carrera et al. (2015) have shown that LDASs can use a small ensemble to provide good LSVs estimates without experiencing the traditional undersampling issues or spurious ensemble covariances. However, if we take into account covariances between patches or between grid cells, this would be a different story. Nevertheless those two caveats can be overcome. Inflation aims to compensate undersampling by artificially inflate the ensemble spread. Approaches have been built to estimate inflation (under the form of a multiplicative coefficient). Anderson (2009) has proposed to add inflation as a parameter in the control vector leading to inflation being updated at each EnKF analysis. Bauser et al. (2018) has successfully applied this approach to a soil hydrology problem. Other approaches based on consistency diagnostics developed by Desroziers et al. (2005) (Li et al., 2009; Miyoshi, 2011) or reformulated EnKFs (Bocquet, 2011; Bocquet and Sakov, 2012) have gained popularity.

Long-range spatial spurious covariances can be filtered out using localisation procedures either by artificially reducing distant spurious correlation (Hamill et al., 2001; Houtekamer and Mitchell, 2001) or by assimilating observations locally (Ott et al., 2004), LDAS-Monde could be seen as an extreme application of the second approach. Localisation procedures are very efficient and are routinely used for a wide range of application.

Unfortunately, the problem of potentially spurious covariances between patches remains as we would need to fix a criterion to determine which covariance has to be reduced. Recently Farchi and Bocquet (2019) has proposed a localisation procedure based on augmented ensembles. Such formulation allows a covariance localisation not based on spatial criteria and could be used to include covariances between patches in LDAS-Monde EnSRF.

6 Conclusions

In this paper, we have adapted the Ensemble Square Root Filter used by Fairbairn et al. (2015) to the context of the joint assimilation of surface soil moisture and leaf area index within LDAS-Monde. The validity of our approach has then be assessed over the Euro-Mediterranean region for the period 2008 – 2017 and compared to a Simplified Extended Kalman Filter, that is routinely used in LDAS-Monde. Results shows that the EnSRF provides estimates of LAI of a similar quality to the SEKF. Estimated EnSRF surface soil moistures tend to get closer to observations than their SEKF counterparts. We also have examined the impact of EnSRF on controlled soil moisture for deeper soil layers. For soil moisture in near-surface layers (4–20 cm depth), analysis increments are similar for both approaches but EnSRF estimates tend to be wetter especially for arid places due to a bias introduced by the model error. For deeper layers (20–80 cm depth), SEKF and EnSRF estimates of soil moisture are similar but are obtained through different mechanisms. While drier soil moisture in SEKF is obtained through the model by transfering information from updated soil moisture in (near-)surface, the EnSRF produces those estimates partly because of the data assimilation routine itself, acting like a bias correction procedure for those layers to compensate for the wet model bias via the correlations between soil moisture in deeper layers and surface soil moisture and LAI. Finally, validation of

https://doi.org/10.5194/hess-2019-391
Preprint. Discussion started: 20 August 2019

our approach has been carried out using datasets of evapotranspiration, gross primary production and river discharges, showing a moderate positive impact for the two previous but a marked positive one for the latter. While involving a crude model error, this paper shows the potential of the EnSRF within LDAS-Monde and constitutes a good basis for further developments.

One limitation of assimilating LAI is that LAI products are only available every 10 days (for CGLS products) making their estimates being correctly updated every ten days (assimilating surface soil moisture has a negligible impact on LAI). LDAS-Monde would benefit from having observations linked to vegetation available every day. This is the case of radar backscatter coefficients as shown by Lievens et al. (2017) and Shamambo et al. (2019) that are already used in our system through the assimilated ASCAT-derived soil water indices. The development of an observation operator linking surface soil moisture and LAI to those coefficients is currently under development at CNRM. Once fully tested, it should, hopefully, provide daily indirect observations of LAI and improve LDAS-Monde daily updates of LAI and soil moisture.

Code availability. LDAS-Monde is a part of the ISBA land surface model and is available as open source via the surface modelling platform called SURFEX. SURFEX can be downloaded freely at http://www.umr-cnrm.fr/surfex/ using a CECILL-C Licence (a French equivalent to the L-GPL licence; http://www.cecill.info/licences/Licence_CeCILL-C_V1-en.txt). It is updated at a relatively low frequency (every 3 to 6 months). If more frequent updates are needed, or if what is required is not in Open-SURFEX (DrHOOK, FA/LFI formats, GAUSSIAN grid), you are invited to follow the procedure to get a SVN account and to access real-time modifications of the code (see the instructions at the first link). The developments presented in this study stemmed on SURFEX version 8.1. LDAS-Monde technical documentation and contact point are freely available at: https://opensource.umr-cnrm.fr/projects/openldasmonde/files

Author contributions. Conceptualization, BB, CA; Investigation, BB; Methodology, BB; Writing—original draft, BB; Writing—review and editing, All

Competing interests. The authors declare no conflict of interest.

Acknowledgements. Results were generated using the Copernicus Climate Change Service Information, 2017. The Authors would like to thanks the Copernicus Global Land Service for providing the satellite derived Leaf Area Index and Surface Soil Moisture.

https://doi.org/10.5194/hess-2019-391
Preprint. Discussion started: 20 August 2019

References

Albergel, C., Rüdiger, C., Pellarin, T., Calvet, J.-C., Fritz, N., Froissard, F., Suquia, D., Petitpa, A., Piguet, B. and Martin, E.: From near-surface to root-zone soil moisture using an exponential filter: An assessment of the method based on in-situ observations and model simulations, Hydrol. Earth Syst. Sci. 12, 1323–1337, 10.5194/hess-12-1323-2008, 2008.

Albergel, C., Calvet, J.-C., Mahfouf, J.-F., Rüdiger, C., Barbu, A. L., Lafont, S., Roujean, J.-L., Walker, J. P., Crapeau, M. and Wigneron, J.-P.: Monitoring of water and carbon fluxes using a land data assimilation system: a case study for southwestern France, Hydrol. Earth. Syst. Sci., 14, 1109-1124, 10.5194/hess-14-1109-2010, 2010.

Albergel, C., Munier S., Leroux, D. J., Dewaele, H., Fairbairn, D., Barbu, A. L, Gelati, E., Dorigo, W., Faroux, S., Meurey, C., Le Moigne, P., Decharme, B., Mahfouf, J.-F. and Calvet, J.-C.: Sequential assimilation of satellite-derived vegetation and soil moisture products using SURFEX_v8.0: LDAS-Monde assessment over the Euro-Mediterranean area, Geosci. Model Dev., 10, 3889–3912, 10.5194/gmd-10-3889-2017, 2017.

Albergel, C., Dutra, E., Munier, S., Calvet, J.-C., Sabater, J. M., de Rosnay, P. and Balsamo, G.: ERA-5 and ERA-Interim driven ISBA land surface model simulations: Which one performs better? Hydrol. Earth Syst. Sci., 22, 3515–3532, 10.5194/hess-22-3515-2018, 2018.

Albergel, C., Munier, S., Bocher, A., Bonan, B., Zheng, Y., Draper, C., Leroux, D. J. and Calvet, J.-C.: LDAS-Monde Sequential Assimilation of Satellite Derived Observations Applied to the Contiguous US: An ERA5 Driven Reanalysis of the Land Surface Variables. Remote Sens., 10, 1627, 10.3390/rs10101627, 2018.

Albergel, C., Dutra, E., Bonan, B., Zheng, Y., Munier, S., Balsamo, G., de Rosnay, P., Sabater, J. M. and Calvet, J.-C.: Monitoring and Forecasting the Impact of the 2018 Summer Heatwave on Vegetation. Remote Sens., 11, 520, 10.3390/rs11050520, 2019.

Anderson, J. L.: An adaptive covariance inflation error correction algorithm for ensemble filters. Tellus A, 59, 210–224, 10.1111/j.1600-0870.2006.00216.x, 2009.

Balsamo, G., Agusti-Panareda, A., Albergel, C., Arduini, G., Beljaars, A., Bidlot, J., Bousserez, N., Boussetta, S., Brown, A., Buizza, R, Buontempo, C., Chevallier, F., Choulga, M., Cloke, H., Cronin, M. F., Dahoui, M., De Rosnay, P., Dirmeyer, P. A., Drusch, M., Dutra, E., Ek, M. B., Gentine, P., Hewitt, H., Keeley, S. P. E., Kerr, Y., Kumar, S., Lupu, C., Mahfouf, J.-F., McNorton, J., Mecklenburg, S., Mogensen, K., Muñoz-Sabater, J., Orth, R., Rabier, R., Reichle, R., Ruston, B., Pappenberger, F., Sandu, I., Seneviratne, S. I., Tietsche, S., Trigo, I. F., Uijlenhoet, R., Wedi, N., Woolway, R. I. and Zeng, X: Satellite and in situ observations for advancing global Earth surface modelling: A review. Remote Sens., 10, 2038, 10.3390/rs10122038, 2018.

Barbu, A. L., Calvet, J.-C., Mahfouf, J.-F., Albergel, C. and Lafont, S.: Assimilation of Soil Wetness Index and Leaf Area Index into the ISBA-A-gs land surface model: grassland case study, Biogeosciences, 8, 1971–1986, 10.5194/bg-8-1971-2011, 2011.

Barbu, A. L., Calvet, J.-C., Mahfouf, J.-F., and Lafont, S.: Integrating ASCAT surface soil moisture and GEOV1 leaf area index into the SURFEX modelling platform: a land data assimilation application over France, Hydrol. Earth Syst. Sci., 18, 173–192, 10.5194/hess-18-173-2014, 2014.

Baret, F., Weiss, M., Lacaze, R., Camacho, F., Makhmared, H., Pacholczyk, P. and Smetse, B.: GEOV1: LAI and FAPAR essential climate variables and FCOVER global time series capitalizing over existing products, Part 1: Principles of development and production, Remote Sens. Environ., 137, 299–309, 10.1016/j.rse.2012.12.027, 2013.

Bartalis, Z., Wagner, W., Naeimi, V., Hasenauer, S., Scipal, K., Bonekamp, H., Figa, J. and Anderson, C.: Initial soil moisture retrievals from the METOP-A Advanced Scatterometer (ASCAT). Geophys. Res. Lett., 34, L20401, 10.1029/2007GL031088, 2007.

https://doi.org/10.5194/hess-2019-391
Preprint. Discussion started: 20 August 2019

Hydrology and Earth System Sciences
Discussions

Bauser, H. H., Berg, D., Klein, O., and Roth, K.: Inflation method for ensemble Kalman filter in soil hydrology, Hydrol. Earth Syst. Sci., 22, 4921-4934, 10.5194/hess-22-4921-2018, 2018.

Berg, D., Bauser, H. H. and Roth, K.: Covariance resampling for particle filter – state and parameter estimation for soil hydrology. Hydrol. Earth Syst. Sci., 23, 1163-1178, 10.5194/hess-23-1163-2019, 2019.

Berry, T. and Sauer, T.: Adaptive ensemble Kalman filtering of non-linear systems. Tellus A, 65, 20331, 10.3402/tellusa.v65i0.20331, 2013.

Bocquet, M.: Ensemble Kalman filtering without the intrinsic need for inflation, Nonlin. Processes Geophys., 18, 735-750, 10.5194/npg-18-735-2011, 2011.

Bocquet, M. and Sakov, P.: Combining inflation-free and iterative ensemble Kalman filters for strongly nonlinear systems, Nonlin. Processes Geophys., 19, 383-399, 10.5194/npg-19-383-2012, 2012.

Bonan, G. B.: Forests and Climate Change: Forcings, Feedbacks, and the Climate Benefits of Forests, Science, 320, 5882, 1444–1449, 10.1126/science.1155121, 2008.

Boone, A., Masson, V., Meyers, T. and Noilhan, J.: The influence of the inclusion of soil freezing on simulations by a soil-vegetation-atmosphere transfer scheme, J. Appl. Meteorol., 39, 1544–1569, 10.1175/1520-0450(2000)039<1544:TIOTIO>2.0.CO;2, 2000.

Bowler, N. E.: On the diagnosis of model error statistics using weak-constraint data assimilation. Q. J. Roy. Meteor. Soc., 143, 1916–1928, 10.1002/qj.3051, 2017.

Blyverket, J., Hamer, P. D., Bertino, L., Albergel, C., Fairbairn, D. and Lahoz, W. A.: An Evaluation of the EnKF vs. EnOI and the Assimilation of SMAP, SMOS and ESA CCI Soil Moisture Data over the Contiguous US. Remote Sens., 11, 478, 10.3390/rs11050478, 2019.

Calvet, J.-C., Noilhan, J., Roujean, J.-L., Bessemoulin, P., Cabelguenne, M., Olioso, A. and Wigneron, J.-P.: An interactive vegetation SVAT model tested against data from six contrasting sites, Agr. Forest Meteorol., 92, 73–95, 10.1016/S0168-1923(98)00091-4, 1998.

Calvet, J.-C., Rivalland, V., Picon-Cochard, C. and Guehl, J.-M.: Modelling forest transpiration and CO2 fluxes—response to soil moisture stress, Agr. Forest Meteorol., 124, 143–156, 10.1016/j.agrformet.2004.01.007, 2004.

Carrera, M. L., Bélair, S. and Bilodeau, B: The Canadian Land Data Assimilation System (CaLDAS): Description and Synthetic Evaluation Study, J. Hydrometeorol., 16, 1293-1314, 10.1175/JHM-D-14-0089.1, 2015.

Corazza, M., Kalnay, E., Patil, D. J., Yang, S.-C., Morss, R., Cai, M., Szunyogh, I., Hunt, B. R., and Yorke, J. A.: Use of the breeding technique to estimate the structure of the analysis "errors of the day", Nonlin. Processes Geophys., 10, 233-243, 10.5194/npg-10-233-2003, 2003.

Decharme, B., Alkama, R., Douville, H., Becker, M. and Cazenave, A.: Global Evaluation of the ISBA-TRIP Continental Hydrological System. Part II: Uncertainties in River Routing Simulation Related to Flow Velocity and Groundwater Storage, J. Hydrometeorol., 11, 601–617, 10.1175/2010JHM1212.1, 2010.

Decharme, B., Boone, A., Delire, C. and Noilhan, J.: Local evaluation of the Interaction between Soil Biosphere Atmosphere soil multilayer diffusion scheme using four pedotransfer functions, J. Geophys. Res., 116, D20126, 10.1029/2011JD016002, 2011.

Decharme, B., Alkama, R., Papa, F., Faroux, S., Douville, H. and Prigent, C.: Global off-line evaluation of the ISBA-TRIP flood model, Clim. Dynam., 38, 1389–1412, 10.1007/s00382-011-1054-9, 2012.

Decharme, B., Martin, E. and Faroux, S.: Reconciling soil thermal and hydrological lower boundary conditions in land surface models, J. Geophys. Res. Atmos., 118, 7819–7834, 10.1002/jgrd.50631, 2013.

Decharme, B., Delire, C., Minvielle, M., Colin, J., Vergnes, J.-P., Alias, A., Saint-Martin, D., Séférian, R., Sénési, S. and Voldoire, A.: Recent changes in the ISBA-CTRIP Land Surface Syste; for use in the CNRM-CM6 climate model and in global off-line hydrological applications, J. Adv. Model Earth Sy., 11, 1207-1252, hrefhttps://doi.org/10.1029/2018MS00154510.1029/2018MS001545, 2019.

https://doi.org/10.5194/hess-2019-391
Preprint. Discussion started: 20 August 2019

Dee, D. P.: Bias and data assimilation, Q. J. Roy. Meteor. Soc., 131, 3323–3343, 10.1256/qj.05.137, 2005.

De Lannoy, G. J. M., de Rosnay, P. and Reichle, R. H.: Soil Moisture Data Assimilation. In Duan, Q., Pappenberger, F., Thielen, J., Wood, A., Cloke, H. and Schaake J. (eds) Handbook of Hydrometeorological Ensemble Forecasting, pp 701–743, Springer, Berlin, Heidelberg, Germany, 10.1007/978-3-642-39925-1_32, 2016.

de Rosnay, P., Drusch, M., Vasiljevic, D., Balsamo, G., Albergel, C. and Isaksen, L.: A simplified Extended Kalman Filter for the global operational soil moisture analysis at ECMWF. Q. J. Roy. Meteor. Soc., 139, 1199–1213, 10.1002/qj.2023, 2013.

Desroziers, G., Berre, L., Chapnik, B. and Poli, P.: Diagnosis of observation, background and analysis-error statistics in observation space. Q. J. Roy. Meteor. Soc., 131, 3385–3396, 10.1256/qj.05.108, 2005.

Dewaele, H., Munier, S., Albergel, C., Planque, C. Laanaia, N., Carrer, D. and Calvet, J.-C.: Parameter optimisation for a better representation of drought by LSMs: inverse modelling vs. sequential data assimilation, Hydrol. Earth. Syst. Sci., 21, 4861–4878, 10.5194/hess-21-4861-2017, 2017.

Dirmeyer, P. A., Peters-Lidard, C. and Balsamo, G.: Land-atmosphere interactions and the water cycle, in: Seamless prediction of the Earth system: from minutes to months, edited by: Brunet, G., Jones, S. and Ruti, P. M., WMO-No. 1156, World Meteorological Organization, Geneva, Switzerland, 145–154, 2015.

Draper, C. S., Mahfouf, J.-F. and Walker, J. P.: An EKF assimilation of AMSR-E soil moisture into the ISBA land surface scheme. J. Geophys. Res., 114, D020104, 10.1029/2008JD011650, 2009.

Draper, C., Mahfouf, J.-F., Calvet, J.-C., Martin, E., and Wagner, W.: Assimilation of ASCAT near-surface soil moisture into the SIM hydrological model over France, Hydrol. Earth Syst. Sci., 15, 3829–3841, 10.5194/hess-15-3829-2011, 2011.

Drusch, M., Wood, E. F. and Gao, H.: Observations operators for the direct assimilation of TRMM microwave imager retrieved soil moisture, Geophys. Res. Lett., 32, L15403, 10.1029/2005GL023623, 2005.

Drusch, M., Scipal, K., de Rosnay, P., Balsamo, G., Andersson, E., Bougeault, P. and Viterbo, P.: Towards a Kalman Filter-based soil moisture analysis system for the operational ECMWF Integrated Forecast System. Geophys. Res. Lett., 36, L10401, 10.1029/2009GL037716, 2009.

Ehsan Bhulyan, M. A., Nikopoulos, E. I., Anagnostou, E. N., Polcher, J., Albergel, C., Dutra, E., Fink, G., Martinez-de la Torre, A. and Munier, S.: Assessment of precipitation error propagation in multi-model global water resource reanalysis. Hydrol. Earth Syst. Sci., 23, 1973-1994, 10.5194/hess-23-1973-2019, 2019.

Fairbairn, D., Barbu, A. L., Mahfouf, J.-F., Calvet, J.-C. and Gelati, E.: Comparing the ensemble and extended Kalman filters for in situ soil moisture assimilation with contrasting conditions, Hydrol. Earth Syst. Sci., 19, 4811–4830, 10.5194/hess-19-4811-2015, 2015.

Fairbairn, D., Barbu, A. L., Napoly, A., Albergel, C., Mahfouf, J.-F. and Calvet, J.-C.: The effect of satellite-derived surface soil moisture and leaf area index land data assimilation on streamflow simulations over France, Hydrol. Earth. Syst. Sci., 21, 2015–2033, 10.5194/hess-21-2015-2017, 2017.

Fang, H., Jiang, C., Li, W., Wei, S., Baret, F., Chen, J. M., Garcia-Haro, J., Liang, S., Liu, R., Myneni, R.B., Pinty, B., Xiao, Z. and Zhu, Z.: Characterization and intercomparison of global moderate resolution leaf area index (LAI) products: Analysis of climatologies and theoretical uncertainties. J. Geophys. Res. Biogeosci., 118, 529–548, 10.1002/jgrg.20051, 2013.

Farchi, A. and Bocquet, B.: On the efficiency of covariance localisation of the ensemble Kalman filter using augmented ensembles. Front. Appl. Math. Stat., 5, 3, 10.3389/fams.2019.00003, 2019.

Faroux, S., Kaptué Tchuenté, A. T., Roujean, J.-L., Masson, V., Martin, E. and Le Moigne, P.: ECOCLIMAP-II/Europe: a twofold database of ecosystems and surface parameters at 1 km resolution based on satellite information for use in land surface, meteorological and climate models, Geosci. Model Dev., 6, 563-582, 10.5194/gmd-6-563-2013, 2013.

https://doi.org/10.5194/hess-2019-391
Preprint. Discussion started: 20 August 2019

Fox, A. M., Hoar, T. J., Anderson, J. L., Arellano, A. F., Smith, W. K., Litvak, M. E., MacBean, N., Schimel, D. S. and Moore, D. J. P.: Evaluation of a Data Assimilation System for Land Surface Models Using CLM4.5. J. Adv. Model Earth Sy., 10, 2471–2494, 10.1002/2018MS001362, 2018.

Gibelin, A.-L., Calvet, J.-C., Roujean, J.-L., Jarlan, L. and Los, S. O.: Ability of the land surface model ISBA-A-gs to simulate leaf area index at the global scale: Comparison with satellites products, J. Geophys. Res., 111, D18102, 10.1029/2005JD006691, 2006.

Hamill, T. M., Whitaker, J. S., and Snyder, C.: Distance-dependent filtering of background error covariance estimates in an ensemble Kalman filter, Mon. Weather Rev., 129, 2776–2790, 10.1175/1520-0493(2001)129<2776%3ADDFOBE>2.0.CO%3B2, 2001.

Hamill, T. M. and Whitaker, J. S.: Accounting for the error due to unresolved scales in ensemble data assimilation: a comparison of different approaches, Mon. Weather Rev., 133, 3132–3147, 10.1175/MWR3020.1, 2005.

Harlim, J., Mahdi, A. and Majda, A. J.: An ensemble Kalman filter for statistical estimation of physics constrained nonlinear regression models. J. Comput. Phys., 257, 782–812, 10.1016/j.jcp.2013.10.025, 2014.

Hersbach, H. and Dee, D.: "ERA-5 reanalysis is in production", ECMWF newsletter, number 147, Spring 2016, p. 7, 2016.

Houtekamer, P. L. and Mitchell, H. L.: A sequential ensemble Kalman filter for atmospheric data assimilation, Mon. Weather Rev., 129, 123–137, 10.1175/1520-0493(2001)129<0123%3AASEKFF>2.0.CO%3B2, 2001.

Ines, A. V., Das, N. N., Hansen, J. W. and Njoku, E.G.: Assimilation of remotely sensed soil moisture and vegetation with a crop simulation model for maize yield prediction. Remote Sens. Environ. 138, 149–164, 10.1016/j.rse.2013.07.018, 2013.

Jarlan, L., Balsamo, G., Lafont, S., Beljaars, A., Calvet, J.-C. and Mougin, E.: Analysis of leaf area index in the ECMWF land surface model and impact on latent heat and carbon fluxes: Application to West Africa. J. Geophys. Res., 113, D24117, 10.1029/2007JD009370, 2008.

Jin, X., Kumar, L., Li, Z., Feng, H., Xu, X., Yang, G. and Wang, J.: A review of data assimilation of remote sensing and crop models, Eur. J. Agron., 92, 141–152, 10.1016/j.eja.2017.11.002, 2018.

Jung, M., Reichstein, M., Schwalm, C. R., Huntingford, C., Sitch, S., Ahlström, A., Arneth, A., Camps-Valls, G., Ciais, P., Friedlingstein, P., Gans, F., Ichii, K., Jain, A. K., Kato, E., Papale, D., Poulter, B., Raduly, B., Rödenbeck, C., Tramontana, G. Viovy, N., Wang, Y. P., Weber, U., Zaehle, S. and Zeng, N.: Compensatory water effects link yearly global land CO 2 sink changes to temperature, Nature, 541, 516–520, 10.1038/nature20780, 2017.

Kumar, S. V., Peters-Lidard, C. D., Mocko, D., Reichle, R. H., Liu, Y., Arsenault, K. R., Xia, Y., Ek, M., Riggs, G., Livneh, B. and Cosh, M: Assimilation of Remotely Sensed Soil Moisture and Snow Depth Retrievals for Drought Estimation. J. Hydrometeorol., 15, 2446–2469, 10.1175/JHM-D-13-0132.1, 2014.

Kumar, S. V., Mocko, D. M., Wang, S., Peters-Lidard, C. D. and Borak, J.: Assimilation of remotely sensed Leaf Area Index into the Noah-MP land surface model: Impacts on water and carbon fluxes and states over the Continental U.S.. J. Hydrometeorol., 10.1175/JHM-D-18-0237.1, 2019.

Lahoz, W. A. and De Lannoy, G. J. M.: Closing the Gaps in Our Knowledge of the Hydrological Cycle over Land: Conceptual Problems. Surv. Geophys., 35, 623–660, 10.1007/s10712-013-9221-7, 2014.

Leroux, D. J., Calvet, J.-C., Munier, S. and Albergel, C.: Using satellite-derived vegetation products to evaluate LDAS-Monde over the Euro-Mediterranean Area, Remote Sens., 10, 1199, 10.3390/rs10081199, 2018.

Lettenmaier, D. P., Alsdorf, D., Dozier, J., Huffman, G.J., Pan, M. and Wood, E.F: Inroads of remote sensing into hydrologic science during the WRR era. Water Resour. Res., 51, 7309–7342, 10.1002/2015WR017616, 2015.

Li, H., Kalnay, E., and Miyoshi, T.: Simultaneous estimation of covariance inflation and observation errors within an ensemble Kalman filter, Q. J. Roy. Meteor. Soc., 135, 523–533, 10.1002/qj.371, 2009.

https://doi.org/10.5194/hess-2019-391
Preprint. Discussion started: 20 August 2019

Lievens, H., Martens, B., Verhoest, N. E. C., Hahn, S., Reichle, R. H. and Miralles, D. G.:Assimilation of global radar backscatter and radiometer brightness temperature observations to improve soil moisture and land evaporation estimates. Remote Sens. Environ., 189, 194–210, 10.1016/j.rse.2016.11.022, 2017.

Ling, X.-L., Fu, C.-B., Yang, Z.-L., and Guo, W.-D.: Comparison of different sequential assimilation algorithms for satellite-derived leaf area index using the Data Assimilation Research Testbed (version Lanai), Geosci. Model Dev., 12, 3119-3133, 10.5194/gmd-12-3119-2019, 2019.

Liu, Q., Reichle, R. H., Bindlish, R., Cosh, M. H., Crow, W. T., de Jeu, R., De Lannoy, G. J. M., Huffman, G. J. and Jackson, T. J.: The Contributions of Precipitation and Soil Moisture Observations to the Skill of Soil Moisture Estimates in a Land Data Assimilation System. J. Hydrometeorol., 12, 750–765, 10.1175/JHM-D-10-05000.1, 2011.

Livings, D. M., Dance, S. L. and Nichols, N. K.: Unbiased Ensemble Square Root Filters. Physica D, 237, 1021–1028, 10.1016/j.physd.2008.01.005, 2008.

Mahfouf, J.-F.: L'analyse dans le sol à Météo-France. Partie 1: Evaluation et perspectives à l'échelle locale, Meteo-France technical report, Toulouse, France, 2007.

Mahfouf, J.-F., Bergaoui, K., Draper, C., Bouyssel, C., Taillefer, F. and Taseva, L.: A comparison of two offline soil analysis schemes for assimilation of screen-level observations, J. Geophys. Res., 114, D08105, 10.1029/2008JD011077, 2009.

Maggioni, V. and Houser, P. R.: Soil Moisture Data Assimilation. In Park, S. and Lu, X. (eds) Data Assimilation for Atmospheric, Oceanic and Hydrologic Applications (Vol. III), pp 195–217, Springer, Cham, Switzerland, 10.1007/978-3-319-43415-5_9, 2017.

Martens, B., Miralles, D. G., Lievens, H., van der Schalie, R., de Jeu, R. A. M., Fernández-Prieto, D., Beck, H. E., Dorigo, W. A. and Verhoest, N. E. C.: GLEAM v3: Satellite-based land evaporation and root-zone soil moisture, Geosci. Model Dev., 10, 1903–1925, 10.5194/gmd-10-1903-2017, 2017.

Masson, V., Le Moigne, P., Martin, E., Faroux, S., Alias, A., Alkama, R., Belamari, S., Barbu, A., Boone, A., Bouyssel, F., Brousseau, P., Brun, E., Calvet, J.-C., Carrer, D., Decharme, B., Delire, C., Donier, S., Essaouini, K., Gibelin, A.-L., Giordani, H., Habets, F., Jidane, M., Kerdraon, G., Kourzeneva, E., Lafaysse, M., Lafont, S., Lebeaupin Brossier, C., Lemonsu, A., Mahfouf, J.-C., Marguinaud, P., Mokhtari, M., Morin, S., Pigeon, G., Salgado, R., Seity, Y., Taillefer, F., Tanguy, G., Tulet, P., Vincendon, B., Vionnet, V. and Voldoire, A.: The SURFEXv7.2 land and ocean surface platform for coupled and offline simulation of earth surface variables and fluxes, Geosci. Model Dev., 6, 929–960, 10.5194/gmd-6-929-2013, 2013.

Miralles, D. G., Holmes, T. R. H., De Jeu, R. A. M., Gash, J. H., Meesters, A. G. C. A. and Dolman, A. J.: Global land-surface evaporation estimated from satellite-based observations. Hydrol. Earth Syst. Sci., 15, 453–469, 10.5194/hess-15-453-2011, 2011.

Miyoshi, T.: The Gaussian Approach to Adaptive Covariance Inflation and Its Implementation with the Local Ensemble Transform Kalman Filter, Mon. Weather Rev., 139, 1519–1535, 10.1175/2010MWR3570.1, 2011.

Munier, S., Polebistki, A., Brown, C., Belaud, G. and Lettenmaier, D. P.: SWOT data assimilation for operational reservoir management on the upper Niger River Basin, Water Resour. Res., 51, 554-575, 10.1002/2014WR016157, 2015.

Noilhan, J. and Planton, S.: A simple parameterization of land surface processes for meteorological models. Mon. Weather Rev., 117, 536–549, 10.1175/1520-0493(1989)117<0536%3AASPOLS>2.0.CO%3B2, 1989.

Noilhan, J. and Mahfouf, J.-F.: The ISBA land surface parameterisation scheme, Global Planetary Change, 13, 145–159, 10.1016/0921-8181(95)00043-7, 1996.

Oki, T. and Sud, Y. C.: Design of Total Runoff Integrating Pathways (TRIP), a global river chanel network, Earth Interact., 2, 1–36, 10.1175/1087-3562(1998)002<0001:DOTRIP>2.3.CO;2, 1998.

https://doi.org/10.5194/hess-2019-391
Preprint. Discussion started: 20 August 2019

Ott, E., Hunt, B. R., Szunyogh, I., Zimin, A. V., Kostelich, E. J., Corazza, M., Kalnay, E., Patil, D. J., and Yorke, A.: A local ensemble Kalman filter for atmospheric data assimilation, Tellus A, 56, 415–428, 10.1111/j.1600-0870.2004.00076.x, 2004.

Pan, M., Wood, E. F., Wojcik, R. and McCabe, M. F.: Estimation of regional terrestrial water cycle using multi-sensor remote sensing observations and data assimilation. Remote Sens. Environ., 112, 1282–1294, 10.1016/j.rse.2007.02.039, 2008.

Pauwels, V. R. N., Verhoest, N. E. C., De Lannoy, G. J. M., Guissard, V., Lucau, C. and Defourny, P.: Optimization of a coupled hydrology–crop growth model through the assimilation of observed soil moisture and leaf area index values using an ensemble Kalman filter. Water Resours. Res., 43, W04421, 10.1029/2006WR004942, 2007.

Plaza, D. A., De Keyser, R., De Lannoy, G. J. M., Giustarini, L., Matgen, P., and Pauwels, V. R. N.: The importance of parameter resampling for soil moisture data assimilation into hydrologic models using the particle filter, Hydrol. Earth Syst. Sci., 16, 375–390, 10.5194/hess-16-375-2012, 2012.

Reichle, R. H., Walker, J. P., Koster, R. D. and Houser, P. R.: Extended versus Ensemble Kalman Filtering for land data assimilation. J. Hydrometeorol., 3, 728–740, 10.1175/1525-7541(2002)003<0728%3AEVEKFF>2.0.CO%3B2, 2002.

Reichle, R. H. and Koster, D.: Bias reduction in short records of satellite soil moisture, Geophys. Res. Lett., 31, L19501, 10.1029/2004GL020938, 2004.

Reichle, R. H., Koster, R. D., Liu, P., Mahanama, S. P. P., Njoku, E. G. and Owe, M.: Comparison and assimilation of global soil moisture retrievals from the Advanced Microwave Scanning Radiometer for the Earth Observing System (AMSR-E) and the Scanning Multichannel Microwave Radiometer (SMMR). J. Geophys. Res. Atmos., 112, D09108, 10.1029/2006JD008033, 2007.

Reichle, R. H., De Lannoy, G. J. M., Forman, B. F., Draper, C. S. and Liu, Q.: Connecting Satellite Observations with Water Cycle Variables Through Land Data Assimilation: Examples Using the NASA GEOS-5 LDAS. Surv. Geophys., 35, 577–606, 10.1007/s10712-013-9220-8, 2014.

Richards, L. A.: Capillary conduction of liquids through porous mediums, Physics, 1, 318–333, 10.1063/1.1745010, 1931.

Rüdiger, C., Albergel, C., Mahfouf, J.-F., Calvet, J.-C., and Walker, J. P.: Evaluation of Jacobians for Leaf Area Index data assimilation with an extended Kalman filter, J. Geophys. Res., 115, D09111, 10.1029/2009JD012912, 2010.

Sabater, J. M., Jarlan, L., Calvet, J.-C., and Boyssel, F.: From near-surface to root-zone soil moisture using different assimilation techniques, J. Hydrometeorol., 8, 194–206, 10.1175/JHM571.1, 2007.

Sabater, J. M., Rüdiger, C., Calvet, J.-C., Fritz, N., Jarlan, L. and Kerr Y.: Joint assimilation of surface soil moisture and LAI observations into a land surface model, Agr. Forest Meteorol., 148, 1362–1373, 10.1016/j.agrformet.2008.04.003, 2008.

Sakov, P. and Oke, P. R.: A deterministic formulation of the Ensemble Kalman Filter: an alternative to ensemble square root filters. Tellus A, 60, 361–371, 10.1111/j.1600-0870.2007.00299.x, 2008.

Sawada, Y., Koike, T. and Walker, J. P.: A land data assimilation system for simultaneous simulation of soil moisture and vegetation dynamics, J. Geophys. Res. Atmos., 120, 5910–5930, 10.1002/2014JD022895, 2015.

Sawada, Y.: Quantifying Drought Propagation from Soil Moisture to Vegetation Dynamics Using a Newly Developed Ecohydrological Land Reanalysis. Remote Sens., 10, 1197, 10.3390/rs10081197, 2018.

Schellekens, J., Dutra, E., Martínez-de la Torre, A., Balsamo, G., van Dijk, A., Sperna Weiland, F., Minvielle, M., Calvet, J.-C., Decharme, B., Eisner, S., Fink, G., Flörke, M., Peßenteiner, S., van Beek, R., Polcher, J., Beck, H., Orth, R., Calton, B., Burke, S., Dorigo, W., and Weedon, G. P.: A global water resources ensemble of hydrological models: the eartH2Observe Tier-1 dataset, Earth Syst. Sci. Data, 9, 389-413, 10.5194/essd-9-389-2017, 2017.

https://doi.org/10.5194/hess-2019-391
Preprint. Discussion started: 20 August 2019

Scipal, K., Drusch, M. and Wagner, W.: Assimilation of a ERS scatterometer derived soil moisture index in the ECMWF numerical weather prediction system, Adv. Water Resour., 31, 1101–1112, 10.1016/j.advwatres.2008.04.013, 2008.

Shamambo, D. C., Bonan, B., Calvet, J.-C., Albergel, C. and Hahn, S.: Interpretation of radar scatterometer observations over land: a case study over southwestern France, Remote Sens., in preparation, 2019.

Stoffelen, A., Aaboe, S., Calvet, J.-C., Cotton, J., De Chiara, G., Figua-Saldana, J., Mouche, A. A., Portabella, M., Scipal, K. and Wagner, W.: Scientific developments and the EPS-SG scatterometer, IEEE J. Sel. Top. Appl., 10, 2086-2097, 10.1109/JSTARS.2017.2696424, 2017.

Tall, M., Albergel, C., Bonan, B., Zheng, Y., Guichard, F., Dramé, M. S., Gaye, A. T., Sintondji, L. O., Hountondji, F. C. C., Nikiema, P. M. and Calvet, J.-C.: Towards a Long-Term Reanalysis of Land Surface Variables over Western Africa: LDAS-Monde Applied over Burkina Faso from 2001 to 2018. Remote Sens., 11, 735, 10.3390/rs11060735, 2019.

Tandeo, P., Ailliot, P., Bocquet, M., Carrassi, A., Miyoshi, T., Pulido, M. and Zhen, Y.: Joint Estimation of Model and Observation Error Covariance Matrices in Data Assimilation: a Review. Mon. Weather Rev., submitted, available at: https://arxiv.org/abs/1807.11221v2, 2018.

Tippett, M. K., Anderson, J. L., Bishop, C. H., Hamill, T. M. and Whitaker, J. S.: Ensemble Square Root Filters. Mon. Weather Rev., 131, 1485–1490, 10.1175/1520-0493(2003)131<1485:ESRF>2.0.CO;2, 2003.

Todling, R.: A lag-1 smoother approach to system-error estimation: sequential method. Q. J. Roy. Meteor. Soc., 141, 1502–1513, 10.1002/qj.2460, 2015.

Tramontana, G., Jung, M., Schwalm, C. R., Ichii, K., Camps-Valls, G., Ráduly, B., Reichstein, M., Arain, M. A., Cescatti, A., Kiely, G., Merbold, L., Serrano-Ortiz, P., Sickert, S., Wolf, S. and Papale, D.: Predicting carbon dioxide and energy fluxes across global FLUXNET sites with regression algorithms, Biogeosciences, 13, 4291-4313, 10.5194/bg-13-4291-2016, 2016.

Vergnes, J.-P. and Decharme, B.: A simple groundwater scheme in the TRIP river routing model: global off-line evaluation against GRACE terrestrial water storage estimates and observed river discharges, Hydrol. Earth. Syst. Sci., 16, 3889–3908, 10.5194/hess-16-3889-2012, 2012.

Vergnes, J.-P., Decharme, B. and Habets, F.: Introduction of groundwater capillary rises using subgrid spatial variability of topography into the ISBA land surface model, J. Geophys. Res. Atmos., 119, 11065–11086, 10.1002/2014JD021573, 2014.

Voldoire, A., Decharme, B., Pianezze, J., Lebeaupin Brossier, C., Sevault, F., Seyfried, L., Garnier, V., Bielli, S., Valcke, S., Alias, A., Accensi, M., Ardhuin, F., Bouin, M.-N., Ducrocq, V., Faroux, S., Giordani, H., Léger, F., Marsaleix, P., Rainaud, R., Redelsperger, J.-L., Richard, E. and Riette, S.: SURFEX v8.0 interface with OASIS3-MCT to couple atmosphere with hydrology, ocean, waves and sea-ice models, from coastal to global scales, Geosci. Model Dev., 10, 4207-4227, 10.5194/gmd-10-4207-2017, 2017.

Vreugdenhil, M., Dorigo, W. A., Wagner, W., de Jeu, R. A. M., Hahn, S. and van Marle, M. J. E.: Analyzing the Vegetation Parameterization in the TU-Wien ASCAT Soil Moisture Retrieval. IEEE T. Geosci. Remote, 54, 6, 3513–31, 10.1109/TGRS.2016.2519842, 2016.

Wagner, W., Lemoine, G. and Rott, H: A method for estimating soil moisture from ERS scatterometer and soil data. Remote Sens. Environ, 70, 191–207, 10.1016/S0034-4257(99)00036-X, 1999.

Whitaker, J. S. and Hamill, T. M.: Ensemble data assimilation without perturbed observations, Mon. Weather Rev., 130, 1913–1924, 10.1175/1520-0493(2002)130<1913:EDAWPO>2.0.CO;2, 2002.

Xiao, Z., Liang, S., Wang, J., Chen, P., Yin, X., Zhang, L. and Song, J.: Use of general regression neural networks for generating the GLASS leaf area index product from time-series MODIS surface reflectance. IEEE Trans. Geosci. Remote, 10.1109/TGRS.2013.2237780, 2013.

Zhang, H., Hendricks Franssen, H.-J., Han, X., Vrugt, J. A., and Vereecken, H.: State and parameter estimation of two land surface models using the ensemble Kalman filter and the particle filter, Hydrol. Earth Syst. Sci., 21, 4927–4958, 10.5194/hess-21-4927-2017, 2017.

https://doi.org/10.5194/hess-2019-391
Preprint. Discussion started: 20 August 2019

Hydrology and Earth System Sciences
Discussions

Table 1. Statistics (Root Mean Square Difference (RMSD), normalized RMSD (nRSMD), correlation (R), and bias) between LDAS-Monde estimates (Model run, SEKF and EnSRF) and observations for CGLS SSM, CGLS LAI, GLEAM Evapotranspiration (E) and FLUXCOM GPP averaged over the Euro-Mediterranean region for the period 2008–2017 (for SSM, LAI and E) or 2008–2013 (for GPP).

Variable	Exp.	RMSD	nRMSD	R	Bias
LAI	Model run	0.880 $m^2.m^{-2}$	0.568	0.593	- 0.020 $m^2.m^{-2}$
	SEKF	0.671 $m^2.m^{-2}$	0.401	0.732	- 0.116 $m^2.m^{-2}$
	EnSRF	0.694 $m^2.m^{-2}$	0.419	0.723	- 0.201 $m^2.m^{-2}$
SSM	Model run	0.035 $m^3.m^{-3}$	0.161	0.544	0.002 $m^3.m^{-3}$
	SEKF	0.032 $m^3.m^{-3}$	0.138	0.652	0.001 $m^3.m^{-3}$
	EnSRF	0.027 $m^3.m^{-3}$	0.117	0.760	0.001 $m^3.m^{-3}$
Evapotranspiration	Model run	0.833 $kg.m^{-2}.day^{-1}$	0.712	0.789	-0.328 $kg.m^{-2}.day^{-1}$
	SEKF	0.778 $kg.m^{-2}.day^{-1}$	0.689	0.803	-0.114 $kg.m^{-2}.day^{-1}$
	EnSRF	0.745 $kg.m^{-2}.day^{-1}$	0.678	0.823	-0.059 $kg.m^{-2}.day^{-1}$
GPP	Model run	1.369 $g(C).m^{-2}.day^{-1}$	0.913	0.784	-0.412 $g(C).m^{-2}.day^{-1}$
	SEKF	1.393 $g(C).m^{-2}.day^{-1}$	0.962	0.786	-0.146 $g(C).m^{-2}.day^{-1}$
	EnSRF	1.344 $g(C).m^{-2}.day^{-1}$	0.908	0.817	-0.105 $g(C).m^{-2}.day^{-1}$

https://doi.org/10.5194/hess-2019-391
Preprint. Discussion started: 20 August 2019

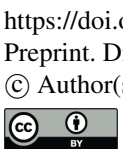

Hydrology and Earth System Sciences
Discussions

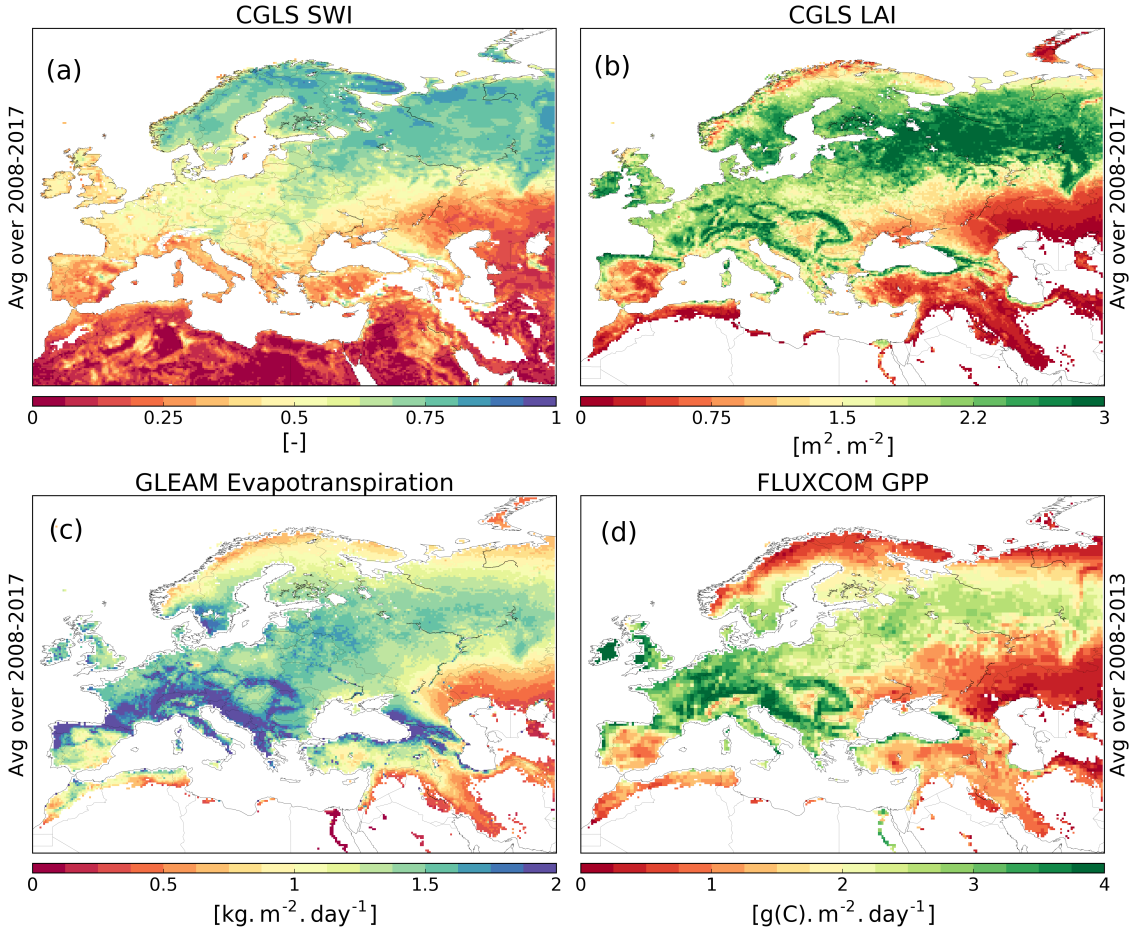

Figure 1. Satellite-derived products of (a) original Soil Water Index (SWI), (b) Leaf Area Index (LAI), (c) evapotranspiration and (d) Gross Primary Production (GPP). They are averaged over 2008–2017 for (a), (b) and (c) and over 2008–2013 for (d).

https://doi.org/10.5194/hess-2019-391
Preprint. Discussion started: 20 August 2019

Hydrology and Earth System Sciences
Discussions

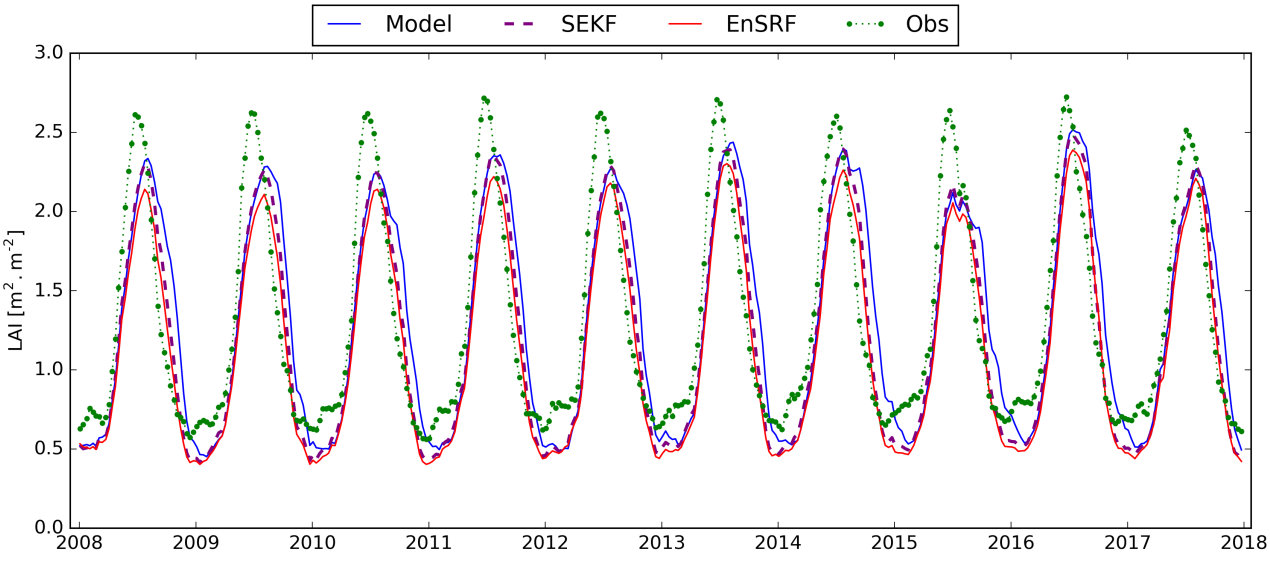

Figure 2. 10-days time series of LAI averaged over the whole domain from the model (blue line), the observations (green dots and dotted line) and analyses obtained with the SEKF (dashed purple line) and the EnSRF (red line) for the period 2008 – 2017.

https://doi.org/10.5194/hess-2019-391
Preprint. Discussion started: 20 August 2019

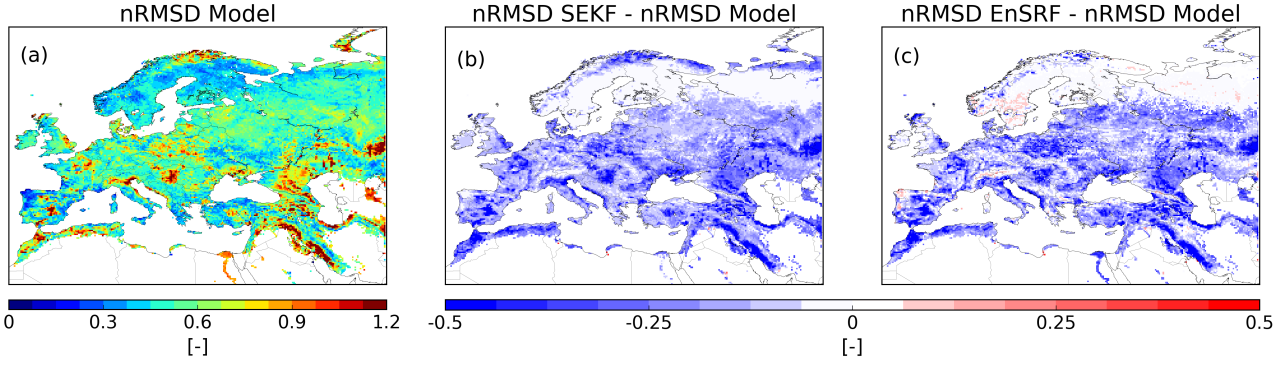

Figure 3. (a) Normalized RMSD (nRMSD) between observed LAI and its model equivalent for the period 2008 – 2017 and difference between nRMSD for SEKF (b) and EnSRF (c) vs nRMSD Model.

https://doi.org/10.5194/hess-2019-391
Preprint. Discussion started: 20 August 2019

Hydrology and Earth System Sciences
Discussions

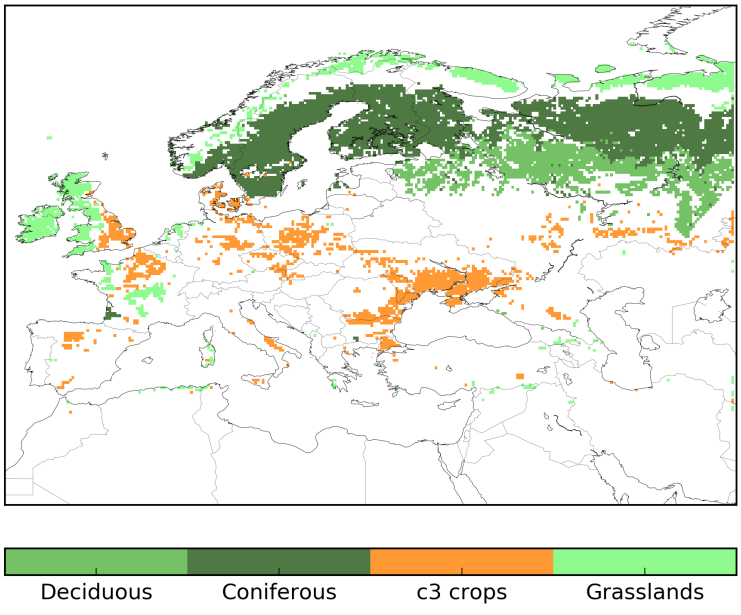

Figure 4. Grid cells of the domain where a vegetation type (or patch) is predominant (patch fraction above 50%). Coniferous trees are dominant for around 15% of the domain that has plants (dark green), deciduous broadleaved trees (green), c3 crops (orange) and grasslands (light green) are in majority for 6% of the domain each.

https://doi.org/10.5194/hess-2019-391
Preprint. Discussion started: 20 August 2019

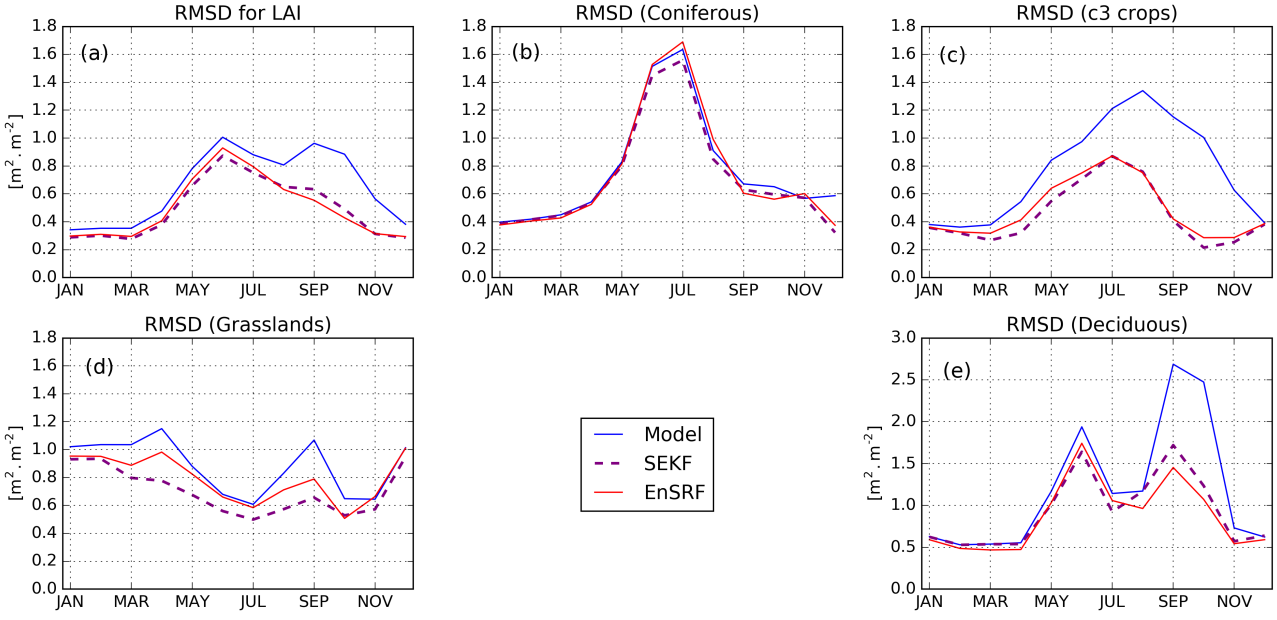

Figure 5. Seasonal RMSD between LAI from observations and the model (blue line), the SEKF analysis (dashed purple line) and the EnSRF analysis (red line) averaged over: (a) the whole domain, and grid cells where (b) coniferous trees, (c) c3 crops, (d) grasslands, (e) deciduous broadleaved trees represent more than 50% of plants for the period 2008 – 2017.

https://doi.org/10.5194/hess-2019-391
Preprint. Discussion started: 20 August 2019

Hydrology and Earth System Sciences
Discussions

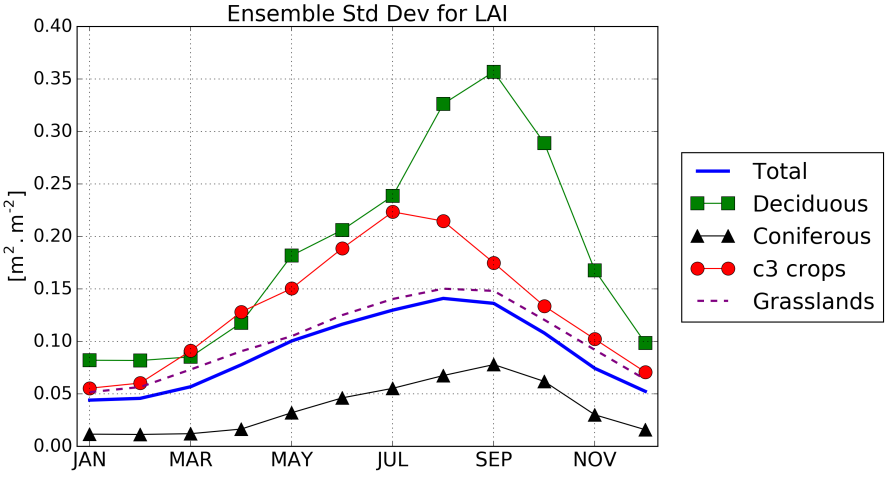

Figure 6. Seasonal standard deviation of the ensemble from the EnSRF averaged over: the whole domain (thick blue line), and grid cells where deciduous broadleaved trees (green squares), coniferous trees (black triangles), c3 crops (red circles) and grasslands (dashed purple line) represent the majority of plants for the period 2008 – 2017.

https://doi.org/10.5194/hess-2019-391
Preprint. Discussion started: 20 August 2019

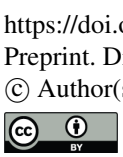

Hydrology and Earth System Sciences
Discussions
Open Access
EGU

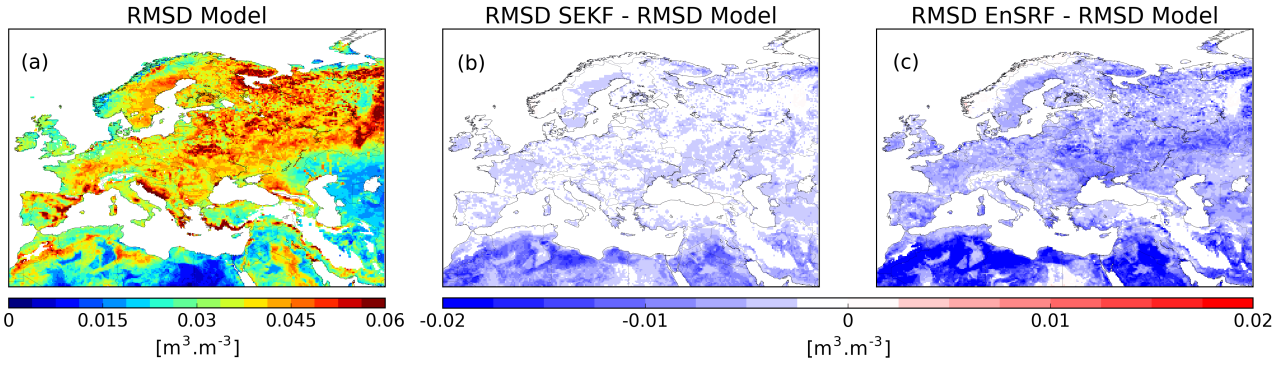

Figure 7. (a) Root mean square difference (RMSD) between observed (rescaled) SSM and its model equivalent for the period 2008 – 2017 and difference between RMSD for SEKF (b) and EnSRF (c) vs RMSD Model.

https://doi.org/10.5194/hess-2019-391
Preprint. Discussion started: 20 August 2019

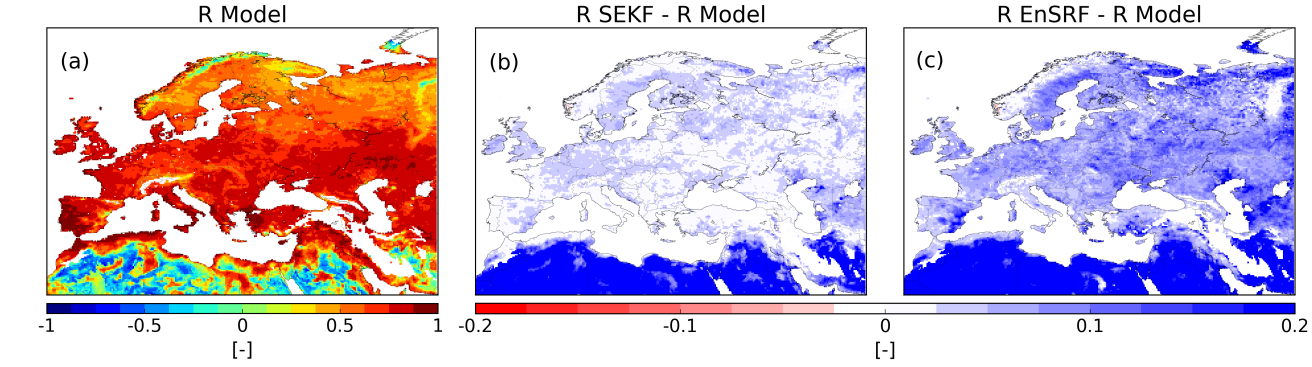

Figure 8. (a) Correlation (R) between observed (rescaled) SSM and its model equivalent for the period 2008 – 2017 and difference between R for SEKF (b) and EnSRF (c) vs R Model.

https://doi.org/10.5194/hess-2019-391
Preprint. Discussion started: 20 August 2019

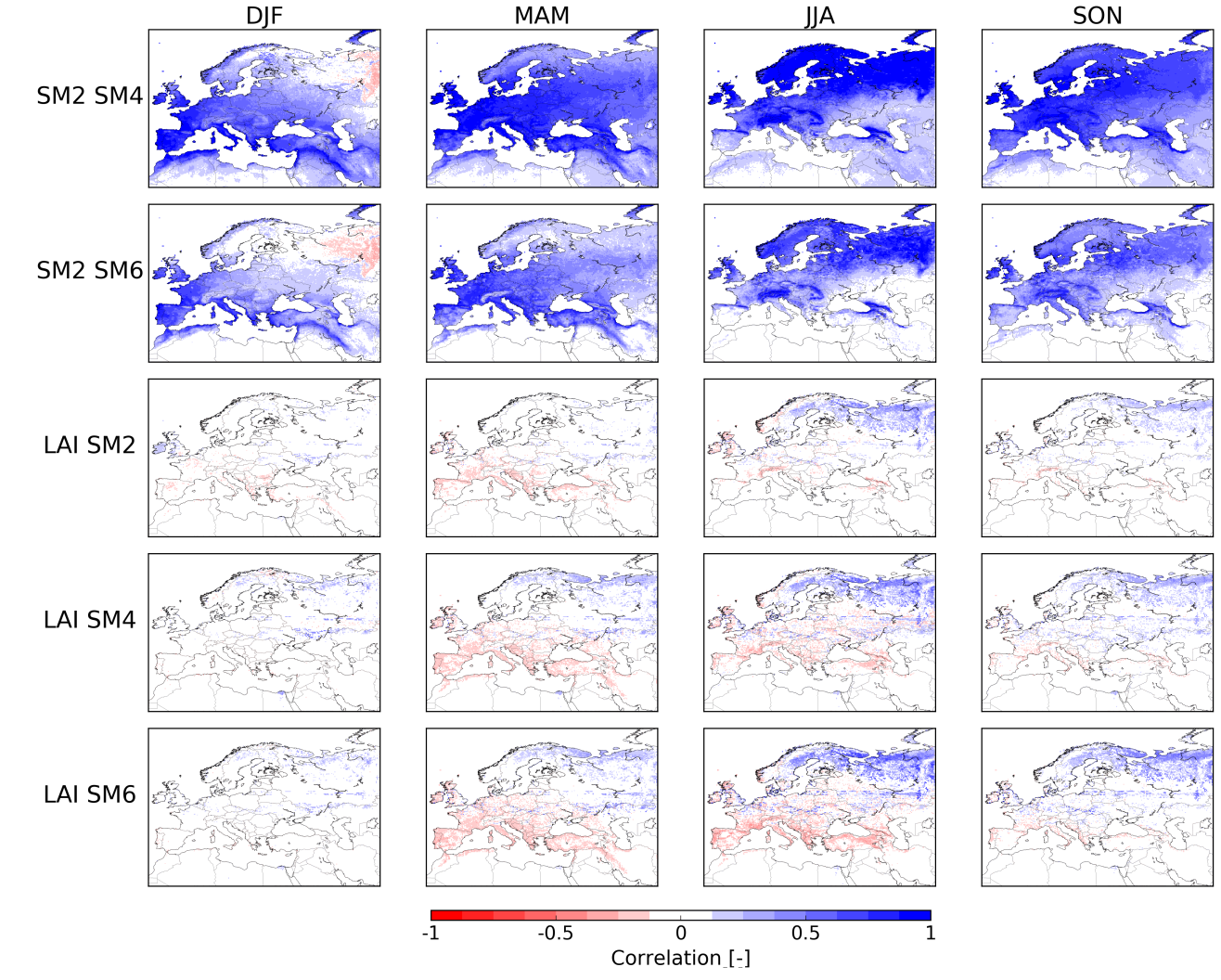

Figure 9. Correlation between the model variables sampled from ensembles and averaged seasonally (DJF=December-January-February, MAM=March-April-May, JJA=June-July-August and SON=September-October-November). From top to bottom, correlation between soil moisture in the second layer (1–4cm, SM2) and the fourth layer (10–20cm, SM4), between SM2 and soil moisture in the sixth layer (40-60cm, SM6), between LAI and SM2, LAI and SM4 and LAI and SM6. Areas is blue exhibit positive correlations, areas in red exhibit anti-correlations.

https://doi.org/10.5194/hess-2019-391
Preprint. Discussion started: 20 August 2019

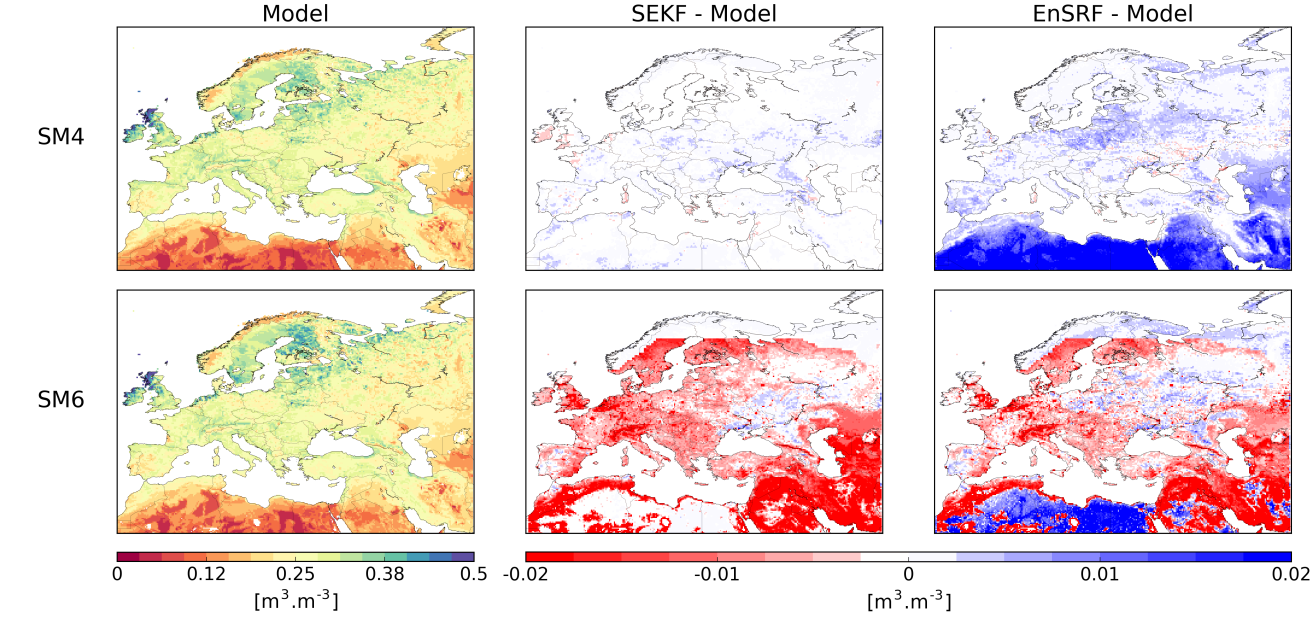

Figure 10. From left to right, averaged soil moisture (fourth layer, 10 – 20 cm, SM4 and sixth layer, 40 – 60 cm, SM6) over 2008 – 2017, averaged analysis impact for SEKF (central) and EnSRF (right).

https://doi.org/10.5194/hess-2019-391
Preprint. Discussion started: 20 August 2019

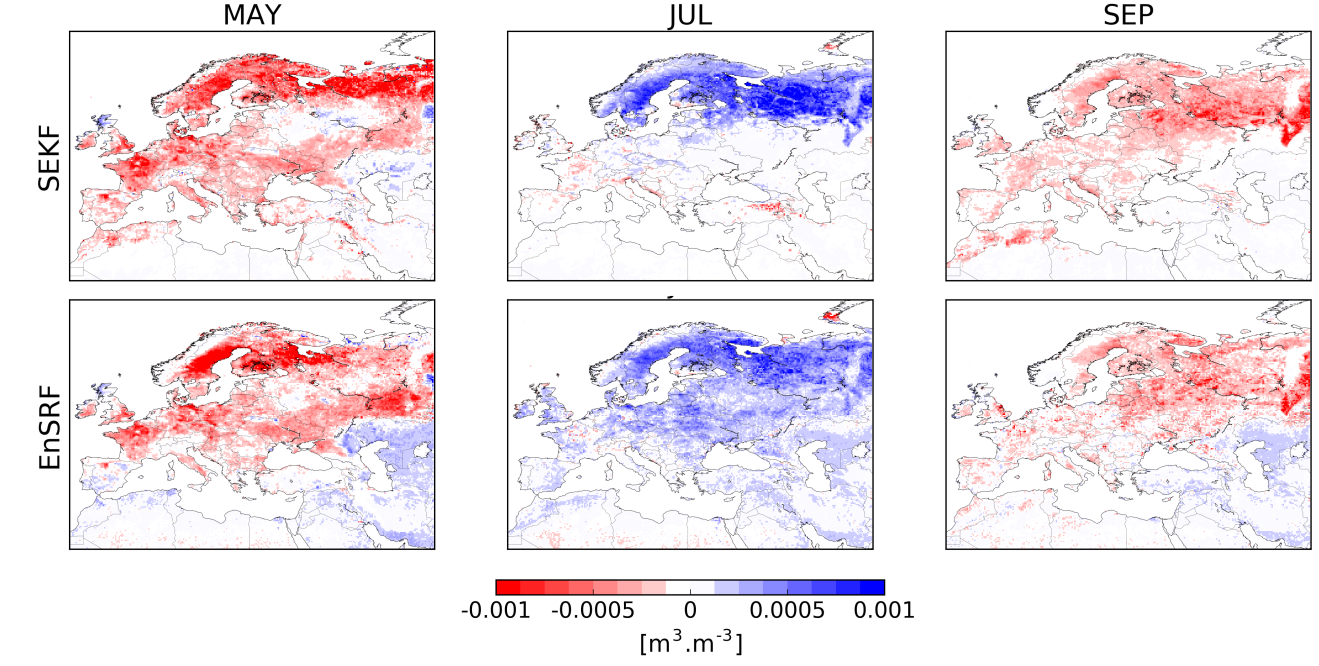

Figure 11. Averaged analysis increments for soil moisture in fourth layer (10 – 20cm, SM4) for SEKF and EnSRF for all months of May (left), July (central) and September (right).

https://doi.org/10.5194/hess-2019-391
Preprint. Discussion started: 20 August 2019

Hydrology and Earth System Sciences
Discussions
Open Access
EGU

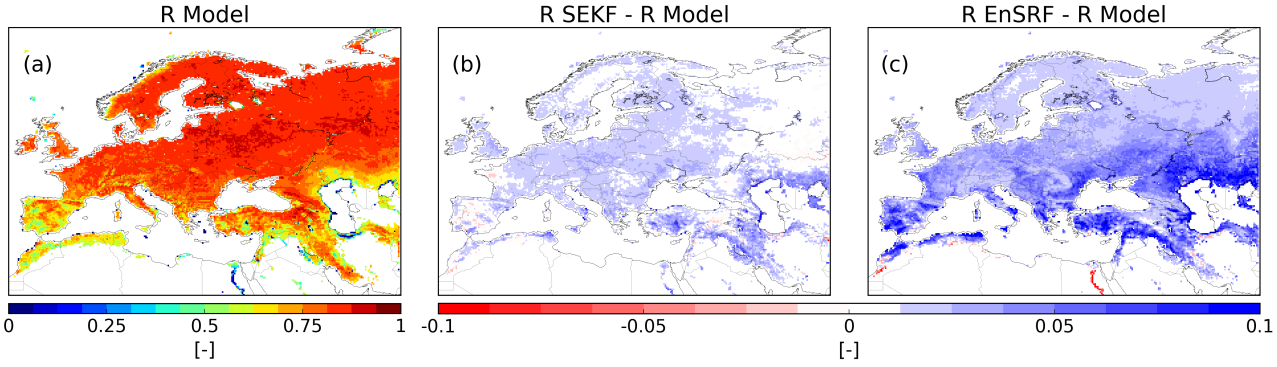

Figure 12. (a) Correlation (R) between observed GLEAM Evapotranspiration and its model equivalent for the period 2008 – 2017 and difference between R for SEKF (b) and EnSRF (c) vs R Model.

https://doi.org/10.5194/hess-2019-391
Preprint. Discussion started: 20 August 2019

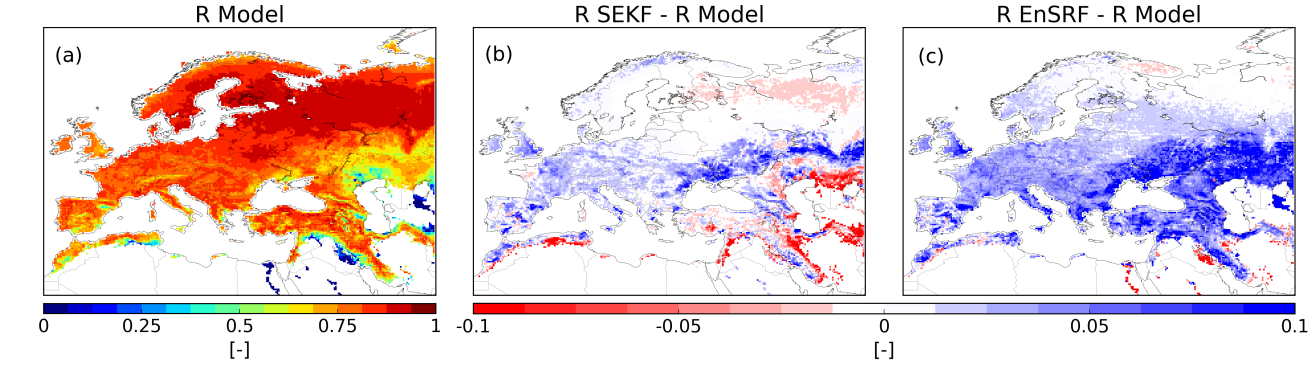

Figure 13. (a) Correlation (R) between observed FLUXCOM gross primary production and its model equivalent for the period 2008 – 2013 and difference between R for SEKF (b) and EnSRF (c) vs R Model.

https://doi.org/10.5194/hess-2019-391
Preprint. Discussion started: 20 August 2019

Hydrology and Earth System Sciences
Discussions

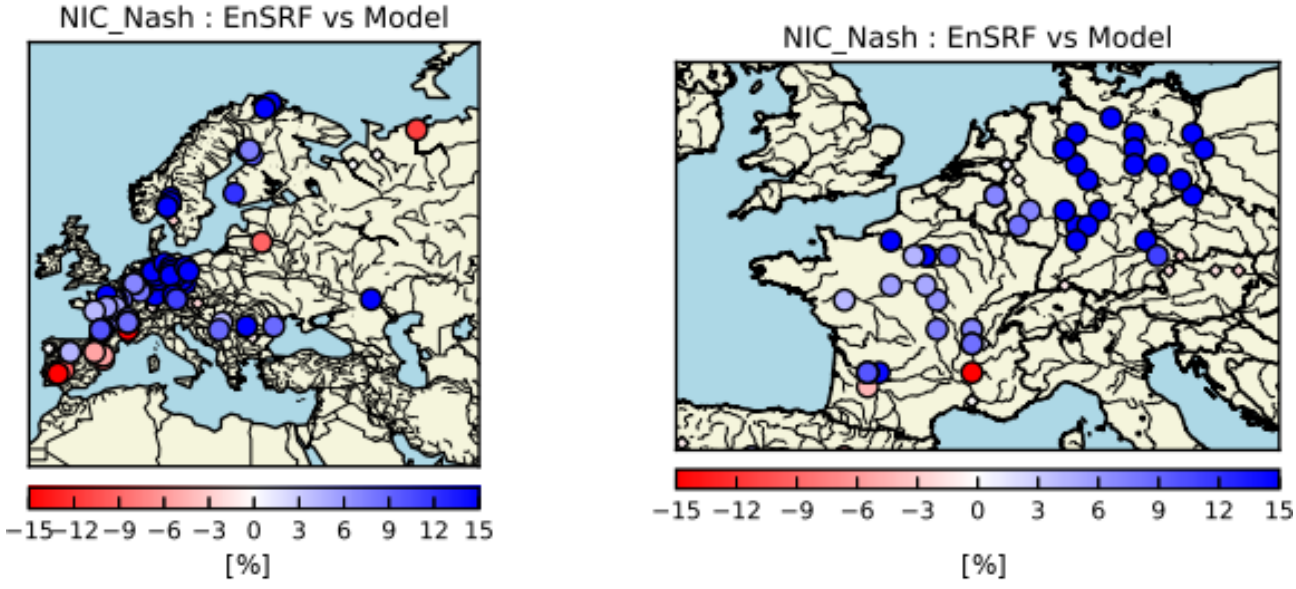

Figure 14. Normalised Information Contribution Index (NIC) assessing the improvement of Nash-Sutcliffe efficiency indices for EnSRF river discharge estimates compared to model counterparts. Blue circles assess a positive impact of DA, red circles a negative impact and small diamonds a neutral impact.